EXACT MODELING OF MULTIPLE ACCESS INTERFERENCE, BER DERIVATION AND A METHOD TO IMPROVE THE PERFORMANCE OF UWB COMMUNICATION SYSTEMS

SOMASUNDARAM NIRANJAYAN

(B.Sc.Eng (Hons.) , University of Moratuwa)

A THESIS SUBMITTED

FOR THE DEGREE OF MASTER OF ENGINEERING

DEPARTMENT OF ELECTRICAL AND COMPUTER ENGINEERING

NATIONAL UNIVERSITY OF SINGAPORE

2004

ACKNOWLEDGEMENT

I devote my special thanks to my mentors Dr. A. Nallanathan and Dr. B. Kannan for their continuous encouragement, support and guidance. Their support extended beyond work, as and when it was needed and helped me to start my professional life in an enlightened path. I am grateful to Institute for Infocom Research (I2R) and Dr. B. Kannan for providing me the financial support and resources throughout the course and for National University of Singapore (NUS) for giving me an opportunity to take up this research project.

I was fortunate to meet and have the friendship of Mahinthan, Suthaharan and Sasiri Yapa in these two years, their friendship made life easy and enjoyable.

I would like to thank my parents, brothers and close friends for their inspiration and encouragement. And, I also like to express my thanks to the four teachers whom I always remember in my life.

Finally, and most importantly, I dedicate my gratitude for my wonderful wife Premila who has sacrificed many things than I ever did, to support me in this mission. Without her moral support, encouragement, cheer-up, and prayers, I would have never been able to accomplish this.

TABLE OF CONTENTS

SUMMARY

Impulse radio is an ultra wideband technique that uses a sequence of sub nanosecond pulses to carry the data. Modulation is achieved by pulse position modulation, pulse amplitude modulation or on-off keying using many pulses per symbol. Multiple access capability is achieved using either direct sequence or time hopping technique. Due to the ability to penetrate through materials and the high resolvability of multipaths with path differential delays on the order of nanoseconds, this technique has greatly attracted the research community recently as a promising candidate for high speed, short range indoor wireless communications. Lack of significant multipath fading helps reducing the fading margins and hence allows low power operation. Therefore, low-cost, low-power and simple transceivers are viable using UWB-IR. And the low power spectral density brings the advantage of license free operation.

Performance measures in wireless communication systems are important in planning the system architecture, link budget and in some cases these help even in choosing the right technology. As far as researchers are concerned, performance measures are important in evaluating and comparing new and existing technologies to choose the right candidate for the purpose of implementation or standardization. It is important to have theoretical tools to evaluate these performance measures accurately, especially the BER which is often much difficult to evaluate. Pure simulation methods are often not computationally efficient and not very useful in analyzing the effects of the system parameters. But, theoretical tools provide a framework to study a system's performance with respect to various system parameters.

In this thesis, we propose exact statistical models for the multiple access interferences of various UWB systems in AWGN channel. These models are derived from basic principles using the geometric properties of UWB-IR signals. We extend the proposed scheme to derive BERs of UWB-IR system in fading channels. We have considered both binary and M-ary modulation schemes in this thesis. Various simulation results are also provided to validate the theoretical results.

We have also proposed a coherent combining technique to improve the performance of an UWB-IR system and its performance is evaluated by comparing it with some other existing systems.

LIST OF FIGURES

NOMENCLATURE

AWGN	Additive White Gaussian Noise
BER	Bit Error Rate
CDF	Cumulative Distribution Function
CF	Characteristic Function
CLT	Central Limit Theorem
DS	Direct Sequence
DS-PAM	Direct Sequence Pulse Amplitude Modulation
FCC	Federal Communications Commission
FF	Flat Fading
GA	Gaussian Approximation
GQR	Gaussian Quadrature Rule
IEEE	Institute of Electrical and Electronics Engineers
IR	Impulse Radio
MAI	Multiple Access Interference
M-PAM	M-ary pulse Pulse Amplitude Modulation
MPI	Multipath Interference
M-PPM	M-ary pulse Position Modulation
MRC	Maximal Ratio Combiner
OOK	On Off Keying
PAM	Pulse Amplitude Modulation
PDF	Probability Density Function
PDP	Power Decay Profile

PPM	Pulse Position Modulation
RX	Receiver
SER	Symbol Error Rate
SIR	Signal to Interference Ratio
SNR	Signal to Noise Ratio
S-RAKE	Selective Rake receiver
TH	Time Hopping
TH-PAM	Time Hopping Pulse Amplitude Modulation
TH-PPM	Time Hopping Pulse Position Modulation
TX	Transmitter
UWB	Ultra Wide Band
WPAN	Wireless Personal Area Network

INTRODUCTION

This chapter begins with a brief introduction to ultra-wideband spread spectrum impulse radio, its advantages and applications. It then describes the motivation for this work and then summarizes the contributions of this thesis.

1.1 Concept and Motivation of UWB communication

High speed multiple access communication over short ranges faces the challenge of multipath fading in indoor wireless channels. Instead of increasing the transmit power, increasing the signal bandwidth to achieve frequency diversity is another way of mitigating the fading effect, [1].

Using sub-nanosecond baseband pulses is a technique to broaden the signal bandwidth. The impulse radio uses this technique to spread the signal energy from near d.c. to a few Gigahertzes [2]. Due to its larger bandwidth the impulsive signal achieve two important qualities, one is the ability to penetrate through materials and the other is the high resolvability of multipaths with path differential delays on the order of nanoseconds [3-4]. Lack of significant multipath fading helps reducing the fading margins and hence allows low transmission-power operation. This carrier-less pulse transmission and low transmission power requirement makes low-cost, low-power and simple transceivers viable using UWB-IR [3]. Furthermore, low transmission power and large bandwidth yield very low transmitted power spectral density. Hence, the

interference to the existing narrowband systems from a UWB device can be reduced significantly [4].

According to the definition of Federal Communications Commission (FCC), USA, a system is characterized as ultra-wideband if the fractional bandwidth $\eta \geq 0.25$; the fractional bandwidth is defined by

$$\eta = \frac{2(f_H - f_L)}{f_H + f_L} \tag{1.1}$$

where f_H and f_L are the upper and lower $10dB$ points of the spectrum respectively. If the center frequency is greater than 6GHz, then the system should have a 10-dB bandwidth larger than or equal to 1.5GHz [5].

In the recent years, UWB-IR is identified as a promising candidate for high speed, short range indoor wireless communications [6-8] and it has created great interest in both academia and industry. Due to the nature of the UWB signal it has applications in areas like, radar imaging, stealth communication, wireless personal area networks (WPANs) , security and defense, positioning and location, vehicular radar systems and intelligent transport.

1.2 Motivation for this research

With the increasing number of wireless technologies and increasing customer expectations and needs in communication, one of the important considerations is the quality of performance that these techniques can deliver in a channel with many impairments. These impairments include thermal noise, fading and shadowing, multiple access interference and interference from external sources. Calculating the

performance measures and adjusting the system parameters in order to optimize various factors like performance, cost, and resource usage are the continuous tasks of communication engineers. Such performance measures are important in planning the system architecture, link budget and in some cases it helps even in choosing the right technology. As far as researchers are concerned, performance measures are important in evaluating and comparing new and existing technologies to choose the right candidate for the purpose of implementation or standardization.

Different performance measures are available to evaluate communication systems, with different levels of ease of evaluation and significance. Firstly, the most common, mostly understood and perhaps the easiest measure is the signal to noise ratio (SNR). Often it is defined at the output of the receiver to give a meaningful representation of the systems ability to recover the information successfully. In fading channels, where the instantaneous SNR is a random variable, the average SNR is used as the measure. Another standard measure in fading channels is the outage probability, which is the probability that the instantaneous error rate is higher than a predefined threshold value. Another measure is the interference rejection ratio which is a measure of system's ability to fight interference. Finally, the most commonly used measure is the bit error rate (BER), which is more informative about a system's capability.

It is important to have theoretical tools to evaluate these performance measures accurately, especially the BER which is often much difficult to evaluate. Pure simulation methods are often not computationally efficient and not very useful in analyzing the effects of the system parameters. But, theoretical tools provide a framework to study a systems performance with respect to various system parameters.

Apart from the problem of performance evaluation, another important issue is performance improvement under the effect of channel impairments. Researchers often try to come out with solutions that can improve the performance, reduce the complexity and cost, and optimize power consumption.

1.3 Contributions of this thesis

This thesis is arranged into 7 chapters, where chapters 3, 4, 5 and 6 are the contributions from this research work. Each of these chapters addresses different problems. Therefore, in order to improve readability, the first section of each chapter is devoted to relevant literature review and introduction.

Chapter 2 describes the signal and channel model used, which develops the framework for the following chapters. It presents the transmitted signal model and receiver signal processing for binary TH-PPM, TH-PAM and DS-PAM systems.

Chapter 3 presents an exact theoretical model for the MAI in AWGN channels for different UWB-IRs: TH-PPM, TH-PAM and DS-PAM. It also presents the derivation of exact BER for these systems based on the proposed MAI model. The BER formulas are verified by simulation results.

In chapter 4, BER of a TH-PPM UWB system in multipath fading channel is derived for a single correlator receiver. The MAI model in chapter 3 is used as a basis to derive the CF of the MAI in fading channels. A new form of numerical approximation for the CF of a lognormal variable is used to derive the CF of the total interference.

Throughout chapter 3 and chapter 4, the performance of binary modulation is considered. In chapter 5 MAI models are derived for M-ary TH-PPM and TH-PAM systems. Based on these models, SER and an upper bound for the SER are derived for TH-PAM and TH-PPM systems respectively.

Chapter 6 presents a novel adaptive transmit array technique to improve the UWB-IR performance in multipath fading channels. It then performs a comparison of this scheme with receiver diversity and analyses the possible use of Rake reception with the proposed technique. The proposed technique is based on coherent combining of electromagnetic signals in space, which improves the SNR significantly.

Finally, the conclusions, remarks and few suggestions for future research work are presented in chapter 7.

The outputs from this work can be found in the following publications:

[1] S. Niranjayan, A. Nallanathan and B. Kannan, "An Adaptive Transmit Diversity Scheme Based on Spatial Signal Combining for TH-PPM UWB", *Proc. Of ISSSTA 2004*, Aug 2004.

[2] S. Niranjayan, A. Nallanathan and B. Kannan, "Delay Tuning Based Transmit Diversity Scheme for TH-PPM UWB: Performance with RAKE Reception and Comparison with Multi RX Schemes", *Proc. of Joint UWBST and IWUWBS 2004*, May 2004.

[3] S. Niranjayan, A. Nallanathan and B. Kannan, “A New Analytical Method for Exact Bit Error Rate Computation of TH-PPM UWB Multiple Access Systems”, *Proc. Of PIMRC 2004*, September 2004.

[4] S. Niranjayan, A. Nallanathan and B. Kannan, “Exact Modeling of Multiple Access Interference and BER Derivation for TH-PPM UWB”, *WCNC 2005*, Accepted for publication.

[5] S. Niranjayan, A. Nallanathan and B. Kannan, “Modeling of Multiple Access Interference and BER Derivation for TH and DS UWB Multiple Access Systems”, *IEEE Transactions on Wireless communications*, Aug. 2004. Submitted.

[6] S. Niranjayan, A. Nallanathan and B. Kannan, “Modeling of Multiple Access Interference and SER Derivation for M-ary TH-PAM /PPM UWB Systems”, *VTC Spring 2005*, Accepted for publication.

SYSTEM AND CHANNEL MODELS

This chapter discusses the signal models and receiver signal processing for TH-PPM, TH-PAM and DS-PAM UWB impulse radios, and the channel model used in this thesis.

2.1 System Models

The IR signal consists of a sequence of mono-pulses, where the multiple access technique can be time hopping (TH) or direct sequence (DS). And, different modulation techniques like PPM, PAM and OOK can be equipped to encode the data on to the pulse sequence. The mono-pulse is a sub nanosecond impulse signal satisfying the spectral requirements set by the regulatory bodies (eg. FCC's spectral mask).

2.1.1 TH-PPM System

In TH technique a sequences of N_s mono-pulses are used to carry the bit information. Each bit duration T_b is divided into N_s frames of length T_f. Each of these frames contains a mono-pulse and the users are identified by the placement pattern of mono-pulses within these frames. Each user u has a unique hopping code C^u which defines this placement pattern, where the i^{th} element of C^u is an integer value such that $C_i^u \in \{0,1,.....N_h - 1\}$. The i^{th} mono-pulse will be offset from the starting of the i^{th} frame by $C_i^u T_c$, where T_c is the hopping step.

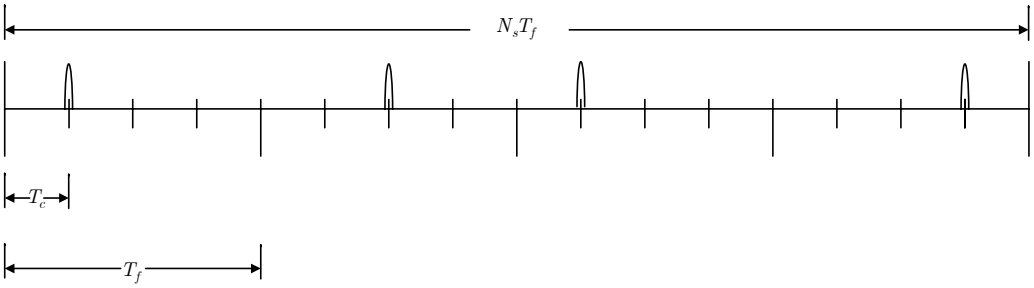

Fig. 2.1 Typical TH –UWB signal example with $Ns = 4$ and $N_h = 4$.

If PPM is employed to encode the binary data, the transmitted signal of the u^{th} user can be written as

$$v_u(t)_{PPM} = \sqrt{E} \sum_{i=0}^{\infty} w\left[t - iT_f - C_i^u T_c - \delta D^u_{\lfloor i/Ns \rfloor}\right] \tag{2.1}$$

where δ is the PPM modulation index and $D_j^u \in \{0,1\}$ is a random variable representing the j^{th} transmitted binary data of user u. Here, $D^u_{\lfloor i/Ns \rfloor}$ represents the data bit over the i^{th} frame and $\lfloor\ \rfloor$- represents the flooring operator. $w(t)$ defines the basic shape of the mono-pulse waveform after modified by the channel and the antenna. The energy of one mono-pulse is given by E and for simplicity $w(t)$ is normalized such that, $\int_{-\infty}^{\infty} w(t)^2 dt = 1$.

A generalized multipath channel model can be expressed by the discrete channel impulse response

$$h(t) = \sum_{l=0}^{L-1} h_l^u \delta(t - \tau_l^u) \tag{2.2}$$

where h_l^u is the channel gain and τ_l^u is the total delay of the l^{th} signal path of user u. The total delay consists of the path delays and the asynchronous access delays between users.

Therefore the received signal is given by

$$r(t)_{PPM} = \sum_{u=0}^{Nu-1} \sum_{l=0}^{L-1} h_l^u v_u (t - \tau_l^u)_{PPM} + n(t) \tag{2.3}$$

where L is the number of significant energy paths, determination of which is based on the channel model adopted. And, $n(t)$ represents the additive white Gaussian noise (AWGN) signal.

Typically the receiver employs RAKE fingers to extract the energy from the multipath components. Each RAKE finger will have a correlator synchronized to a particular path. Since the signal processing in each finger is identical, it is enough presenting the structure of a single correlator receiver. Extending it to the RAKE receiver is instrumental. The correlating template waveform used for the detection of the j^{th} bit of the 0^{th} (desired) user is given by

$$b_T(t)_{PPM} = \sum_{i=jN_s}^{(j+1)N_s-1} b\left(t - iT_f - C_i^0 T_c\right), \tag{2.4}$$

where

$$b(t) = w(t) - w(t - \delta). \tag{2.5}$$

The decision variable at the output of the correlator detector, which extracts the energy from the first path, is given by

$$r_{PPM} = \int_{jT_b}^{(j+1)T_b} h_0^0 b_T (t - \tau_0^0)_{PPM} r(t)_{PPM} dt = s_{PPM} + I_{PPM} + n_{PPM} \tag{2.6}$$

where $T_b = N_s T_f$ is the symbol period, n_{PPM} is the filtered noise and s_{PPM} is the desired signal component where, $s_{PPM} = \left(h_0^0\right)^2 (-1)^{D_j^0} N_s \sqrt{E} \int_{-\infty}^{\infty} w(t) b(t) dt$.

The MAI component I_{PPM} is given by

$$I_{PPM} = \int_{jT_b}^{(j+1)T_b} h_0^0 \, b_T(t-\tau_0^0)_{PPM} \sum_{u=0}^{N_u-1} \sum_{\substack{l=0 \\ l=1 \, if \, u=0}}^{L-1} h_l^u v_u(t-\tau_l^u) dt \,. \tag{2.7}$$

Finally, the decision rule used by the detector is

$$"Decide" \begin{cases} D_j = 0 \Leftrightarrow r_{PPM} > 0 \\ D_j = 1 \Leftrightarrow r_{PPM} < 0 \end{cases}. \tag{2.8}$$

2.1.2 TH-PAM System

In a binary TH-PAM system the data is encoded on to the pulse stream by inverting the polarity of the pulses whenever a bit '1' is transmitted. Using the same notations as in TH-PPM, the TH-PAM transmitted signal can be written as

$$v_u(t)_{PAM} = \sqrt{E} \sum_{i=0}^{\infty} (-1)^{D^u_{\lfloor i/Ns \rfloor}} w\left[t - iT_f - C_i^u T_c\right]. \tag{2.9}$$

For the channel impulse response in (2.2) the received signal can be written as

$$r(t)_{PAM} = \sum_{u=0}^{Nu-1} \sum_{l=0}^{L-1} h_l^u \, v_u(t-\tau_l^u)_{PAM} + n(t). \tag{2.10}$$

The PAM template waveform for the detection of the j^{th} bit of the 0^{th} user becomes

$$b_T(t)_{PAM} = \sum_{i=jN_s}^{(j+1)N_s-1} w\left(t - iT_f - C_i^0 T_c\right). \tag{2.11}$$

Considering that the detection is done by extracting the energy from the first arrival path, the decision variable is given by

$$r_{PAM} = \int_{jT_b}^{(j+1)T_b} h_0^0 b_T(t-\tau_0^0)_{PAM} \times r(t)_{PAM} dt = s_{PAM} + I_{PAM} + n_{PAM}, \tag{2.12}$$

where the MAI term I_{PAM} is given by

$$I_{PAM} = \int_{jT_b}^{(j+1)T_b} h_0^0 \, b_T(t-\tau_1^0)_{PAM} \sum_{u=0}^{N_u-1} \sum_{\substack{l=0 \\ l=1 \, if \, u=0}}^{L-1} h_l^u v_u(t-\tau_l^u)_{PAM} \, dt \, . \tag{2.13}$$

The signal component s_{PAM} is equal to $\left(h_0^0\right)^2 (-1)^{D_j^0} N_s \sqrt{E}$ and the decision rule is equal to that of the PPM case.

2.1.3 DS-PAM System

In DS-PAM each bit interval is divided in to N_s chips of length T_c. Each chip will have a mono-pulse weighted by $a_i^u \in \{\pm 1\}$ which represents the spreading sequence assigned to user u. Using similar notations a binary DS-PAM signal can be expressed as

$$v_u(t)_{DS-PAM} = \sqrt{E} \, (-1)^{D_{\lfloor i/N_s \rfloor}^u} \sum_{i=0}^{\infty} a_i^u w\left[t - iT_c\right], \tag{2.14}$$

where $T_b = N_s T_c$ is the bit interval. Modulation is achieved by multiplying the pulse stream over a bit interval by either 1 or -1 to represent bits 0 or 1 respectively.

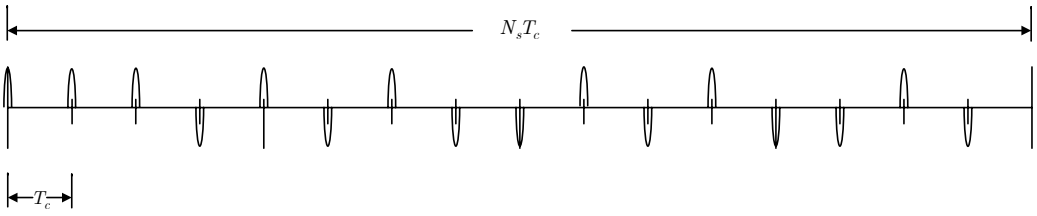

Fig. 2.2 Typical DS-UWB signal example with $N_s = 16$.

Now the received signal is given by

$$r(t)_{DS-PAM} = \sum_{u=0}^{Nu-1} \sum_{l=0}^{L-1} h_l^u v_u(t-\tau_l^u)_{DS-PAM} + n(t). \tag{2.15}$$

Corresponding template waveform of the correlator detector to detect the j^{th} bit of the 0^{th} user is given by

$$b_T(t)_{DS-PAM} = \sum_{i=jN_s}^{(j+1)Ns-1} a_i^0 w[t - iT_c]. \quad (2.16)$$

Therefore the decision variable is given by

$$r_{DS-PAM} = \int_{jT_b}^{(j+1)T_b} h_0^0 b_T(t-\tau_0^0)_{DS-PAM} r(t)_{DS-PAM} dt = s_{DS-PAM} + I_{DS-PAM} + n_{DS-PAM}, \quad (2.17)$$

where the interference term I_{DS-PAM} can be expressed as

$$I_{DS-PAM} = \int_{jT_b}^{(j+1)T_b} h_0^0 b_T(t-\tau_1^0)_{DS-PAM} \sum_{u=0}^{N_u-1} \sum_{\substack{l=0 \\ l=1 if u=0}}^{L-1} h_l^u v_u(t-\tau_l^u)_{DS-PAM} dt. \quad (2.18)$$

s_{DS-PAM} is equivalent to s_{PAM} and the decision rule for DS-PAM is given by

$$"Decide" \begin{cases} D_j = 0 \Leftrightarrow r_{DS-PAM} > 0 \\ D_j = 1 \Leftrightarrow r_{DS-PAM} < 0 \end{cases}. \quad (2.19)$$

2.2 Channel model

The channel model in [9,10] has been recommended by the standardization group, IEEE 802.15.3a, as the model for the evaluation of the proposals for UWB standardization activities. We make use of this channel model and in some cases we simplify the model to have closed form solutions. UWB indoor propagation studies show that the multipath arrivals are clustered rather than in a continuum [9-11]. These clusters are resulting from the larger structural variations of the building, whereas the rays within a cluster are from smaller variations [11]. In order to reflect this clustering phenomenon, the popular Saleh-Valenzuela (S-V) model [12] is used as the basis for the IEEE802.15.3a channel characterization activities. However, slight modifications

are needed since the original S-V model considers a comparatively lower bandwidth channel which is on the order of 100MHz.

The multipath gain magnitude statistics in a UWB channel is no longer Rayleigh or Rician as it is the case of narrowband channels in communications. Due to the fine resolvability, only a few multipath components may overlap within each resolvable delay bin. Therefore invoking the 'central limit theorem' (CLT), which is the basis for Raileigh and Rician models, is no longer valid. The measurement studies further confirm this and the gain magnitude statistics is found to follow either a lognormal or Nakagami distribution [9, 10, 13, 14] . Therefore the IEEE channel model recommends lognormal distribution to model the multipath gain magnitude. In addition to that, cluster fading and fading of rays within each cluster are assumed to be independent.

The multipath model consists of the following discrete time impulse response:

$$h(t) = X\sum_{k=0}^{K-1}\sum_{l=0}^{L-1}\psi_{l,k}\,\delta\left(t - T_k - T_{l,k}\right) \tag{2.20}$$

where $\psi_{l,k}$ is the multipath gain coefficient, T_k is the delay of the k^{th} cluster, $T_{l,k}$ is the delay of the l^{th} path within a cluster relative to the first path, X represents the lognormal shadowing and $\delta(.)$ is the Dirac delta function. The arrival times of rays and clusters are modeled by Poisson processes, thus the distribution of T_k and $T_{l,k}$ can be given by the following conditional density functions,

$$\begin{aligned} P(T_k / T_{k-1}) &= \Lambda e^{-\Lambda(T_k - T_{k-1})}, \quad k > 0 \\ P(T_{l,k} / T_{l-1,k}) &= \Theta e^{-\Theta(T_{l,k} - T_{l-1,k})}, \quad l > 0 \end{aligned} \tag{2.21}$$

where Λ, Θ respectively represent the cluster arrival rate and ray arrival rate. The gain coefficient $\psi_{k,l}$ has the following definition

$$\psi_{l,k} = p_{l,k}\xi_k\beta_{l,k} \tag{2.22}$$

In which $\left|\xi_k\beta_{l,k}\right|$ follows a lognormal distribution and can be expressed by $\left|\xi_k\beta_{l,k}\right| = 10^{\left(\mu_{l,k}+\chi_1+\chi_2\right)/20}$, where $\chi_1 \propto N\left(0,\ \sigma_{\chi_1}^2\right)$ and $\chi_2 \propto N\left(0,\ \sigma_{\chi_2}^2\right)$ are corresponding to the independent fading on each cluster and ray respectively. The equiprobable signal inversions are represented by $p_{l,k} \in \{-1,1\}$.

The power delay profile can be represented as $E\left[\left|\xi_k\beta_{l,k}\right|^2\right] = \upsilon_0\, e^{-T_k/\Gamma}\, e^{-T_{l,k}/\theta}$ where υ_0 is the mean energy of the first path of the first cluster and Γ and θ denote the cluster and ray decay factor respectively. The $\mu_{l,k}$ is given by

$$\mu_{l,k} = \frac{10\ln\left(\upsilon_0\right) - 10T_k/\Gamma - 10T_{l,k}/\theta}{\ln(10)} - \frac{\left(\sigma_{\chi_1}^2 + \sigma_{\chi_2}^2\right)\ln(10)}{20}. \tag{2.23}$$

Since the term X captures the lognormal shadowing of the total multipath energy, the coefficients $\psi_{k,l}$ are normalized to unity. The shadowing is characterized by $20\log_{10}(X) \propto N\left(0,\sigma_X^2\right)$ where σ_X is the standard deviation of lognormal shadowing in dB.

EXACT PERFORMANCE ANALYSIS IN AWGN CHANNELS

This chapter provides the solution for a popular problem in the area of UWB IR performance analysis. That is the exact modeling of multiple access interference. This chapter presents the motivation for this work, statistical modeling of MAI for TH-PPM, TH-PAM and DS-PAM UWB-IR systems in AWGN channel; and analytical derivations of BERs using characteristic function method.

3.1 Introduction and motivation

Theoretical tools for evaluating the performance in terms of bit error rate are important in simplifying the system design and deployment tasks. In the recent past, such theoretical evaluations of the BER of various UWB systems have been reported under different conditions and assumptions.

Single user in AWGN channel was considered in [15], and [16], and under these conditions, the problem is straight forward and the BER can be represented by the Gaussian Q-function (or the Gaussian tail probability) exactly.

Single user in multipath fading channel case was handled in [17-25]; and the problem is somewhat analytically tractable even for RAKE receivers due to the absence of MAI.

System performance in AWGN channels considering multiple access interference

was addressed in [4], [16], [26-28], where the MAI is modeled as a Gaussian random variable (generally known as Gaussian Approximation (GA)). As it was clearly stated in [27], GA was taken on the decision variable (i.e the correlator output) not on the received waveform. Because only a few pulses may arrive simultaneously at a given time slot, invoking the central limit theorem (CLT) on the received signal is not viable. With the GA assumption, the problem was simplified and became tractable and lead to a simple closed form solution.

In multiuser multipath fading conditions, either the GA was used in deriving the average BER [16], [29] or the performance evaluation was based entirely on Monte-Carlo simulations [30].

The accuracy of the GA was questioned and proven to be highly over-estimating the performance of TH systems [31-33]. Failure of GA was due to the concentration of interference probability density function (PDF) at some special values and its non-smooth nature [32].

For multiuser AWGN channel, some non-GA alternative methods were proposed or used in [32-37]. In [32], analysis was performed for a synchronous TH-UWB and an approximated PDF of the interference was used for asynchronous case. An approach assuming rectangular mono-pulse shape has been presented in [33] and [37] for two different modulation schemes. A semi analytical method was introduced in [36], which uses the Gaussian quadrature rule (GQR) to perform the integration on the conditional BER to obtain the average BER. In [35], another approach was introduced using an approximate characteristic function. Another characteristic function based approach

was introduced in [34] with more accurate modeling of the MAI.

These derivations are either approximate or pulse shape dependant or semi analytical and hence do not exactly model the MAI for an arbitrary pulse shape. In [34], the modeling of the ancillary variable [34, eq. (10)] was not accurate for realistic UWB environments as it was not considering full asynchronous access of the users. In [35], a fully asynchronous system was considered, but as mentioned above it did not exactly model the MAI.

Also in [32-34] & [37] it was assumed that the interferences caused by individual pulses residing in different frames were independent, and thus the total interference over one symbol duration was defined as a sum of number of independent and identically distributed (i.i.d.) random variables. But in reality, there exist a certain dependency among these variables; therefore the sum of the interferences from all the frames should be modeled directly from the basic principles without the i.i.d. assumption at the beginning.

In [38], BER analysis for TH-UWB under full asynchronous access condition was performed by modeling the total interference of one bit duration directly from basic principles and the exact BER equations were derived for orthogonal PPM modulation schemes.

The theoretical analysis of BER in AWGN channels is important in both outdoor and indoor environments. In outdoor, it can be used as a good estimate for the system BER performance since the effect of multipaths is much less, and in indoor channels it

can be used as the preliminary step in developing the analysis towards fading channels.

3.2 Multiple access interference model

The impulse wave $w(t)$ can be any narrow pulse waveform satisfying the spectral requirements. The autocorrelation function of $w(t)$ and the cross correlation function $R_{wb}(\tau)$ are respectively defined as

$$R_{ww}(\tau) = \int_{-\infty}^{\infty} w(t)w(t-\tau)dt \ , \tag{3.1}$$

$$R_{wb}(\tau) = \int_{-\infty}^{\infty} w(t)b(t-\tau)dt \, , \tag{3.2}$$

where $b(t)$ represents a template pulse (in PPM, template pulse refers to one of the N_s bi-pulse waveforms of $b_T(t)_{PPM}$ and in PAM it is a mono-pulse). $R_{wb}(\tau)$ is equivalent to $R_{ww}(\tau) - R_{ww}(\tau - \delta)$ for PPM modulation and to $R_{ww}(\tau)$ for PAM modulation. If τ_m is the impulse width of $w(t)$, both $R_{ww}(\tau)$ and $R_{wb}(\tau)$ will be confined within the ranges $[-\tau_m,\tau_m]$ and $[-(\tau_m + \delta),\tau_m]$, respectively.

The first step in modeling the total MAI is the modeling of the interference contributed by one template pulse, when correlated against the interfering signal, arriving through a single path of an interfering user. This interference related to one template pulse can be modeled by the function $R_{wb}(\tau)$ by attributing the randomness to the variable τ.

3.2.1 Modeling of τ

In [34], the argument of $R_{wb}(.)$ which was named as the ancillary variable, was

implicitly modeled as (let denote it by ψ)

$$\psi = \alpha_u + (c_j^u - c_j^0)T_c + D_j^u \delta \tag{3.3}$$

where α_u was the asynchronous time delay difference between user u and user 0. (wherever applicable user 0 is assumed as the desired user).

This equation actually models the total delay difference between the j^{th} pulses of the u^{th} user signal and the template signal. This modeling is valid if α_u is confined within $\left[-\frac{T_f}{2}, \frac{T_f}{2}\right]$. But in reality the actual range of α_u should be $\left[-\frac{N_s T_f}{2}, \frac{N_s T_f}{2}\right]$, i.e. spanned throughout one bit duration since the users can initiate transmission at any time independent of the access of other users. Secondly, if multipath arrivals are also considered, another additional time variable accounting for the Poisson arrivals [9] will contribute to the total asynchronism. As a result, both will increase the range of ψ and hence, the modeling as in (3.3) will ignore the chances of interference caused by the subsequent pulses in the sequence.

In Fig. 3.2 the small 'ticks' denote the pulse origins. Pulse origins are defined as the points in the time axis that can possibly accommodate a mono-pulse. Therefore, we define τ as the time difference from a template pulse, to its *closest* pulse origin of the interfering signal (Fig. 3.2). With the assumption of a random chip code, the closest pulse origin can have a mono-pulse with a probability $1/N_h$, with N_h being the number of chips in a frame.

Since τ is the distance to the neighboring pulse origin, the maximum value of $|\tau|$ is equal to $\frac{T_c}{2}$. Therefore the range of τ is given by, $\tau \in \left[-\frac{T_c}{2}, \frac{T_c}{2}\right]$. In an AWGN channel

the absolute positioning of pulse origins in the interfering signal's time axis is determined by α_u, T_c, δ, c_i^u and D_j^u.

But, since T_c and δ are much smaller than the range of the uniform random variable α_u, the effect due to the discreteness in the distributions of the chip code and the data bit will be eliminated. Hence, the distribution of τ will eventually become *uniform within the above range* (It should be noted that this uniformity is not an assumption, it is an exact scenario).

In a channel with delays related to Poisson arrivals, the rms (root mean square) delay spread will be much smaller than $N_s T_f$ (generally T_f is set larger than the channels delay spread to avoid inter symbol interference). Therefore the distribution of τ will be approximately uniform even in a multipath channel. This is verified by simulations in Fig. 3.1.

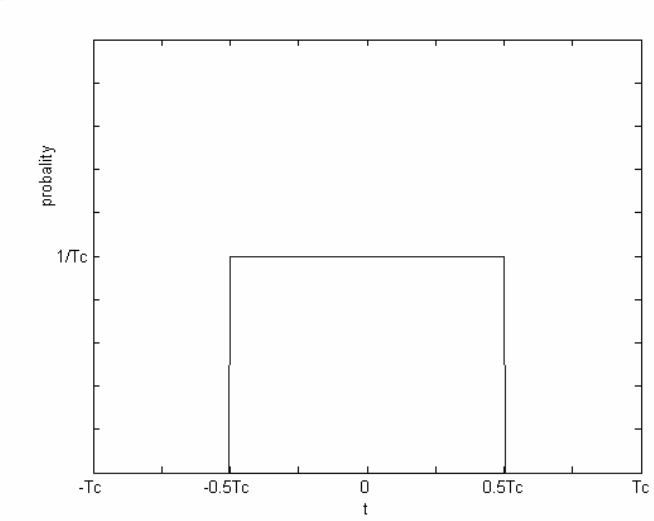

Fig . 3.1 Simulation plot of the distribution of τ for $T_c = 4ns$, in a channel with poisson arrivals with an arrival rate equal to 0.0233.

According to the system model in chapter 2, it is assumed that there is no extra guard time provided between adjacent bits, except the inherent clearance available due to the

chip time T_c. As in [35-36], we also assume that T_f is spanned by an integer number of chip durations, i.e. $T_c = T_f / N_h$.

3.2.2 TH-PPM System

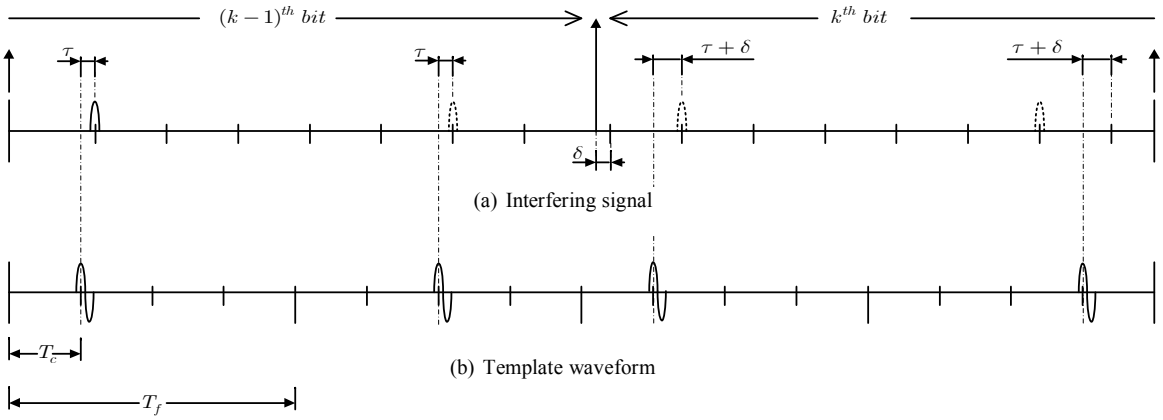

Fig. 3.2 An interfering signal (a) compared against the template waveform (b) of the desired user with $N_s = 4$ and $T_c = T_f / 4$ for TH-PPM. Shown example is for $D_{k-1}D_k$ =01.

Fig. 3.2 depicts one interfering signal against the template waveform of the desired user, throughout a full bit duration for TH-PPM. It should be noted that a maximum of one bit changeover can occur during the considered time window (the interfering signal changes from $(k-1)^{th}$ bit to k^{th} bit). An arbitrary chip pattern is assumed for user 0. The interfering signal is viewed as an infinite sequence of mono-pulses, and its time axis consists of two sets of pulse origins (as marked in the diagram) corresponding to $(k-1)^{th}$ and k^{th} bit durations. And, the elements within each set are equally spaced.

Now let τ be the distance to the closest interfering pulse origin from the first template pulse. Therefore the interference related to the first template pulse is $R_{wb}(\tau)$

with a probability of occurrence $1/N_h$. It can be noted that all pulse origins in the $(k-1)^{th}$ bit are shifted by τ, relative to their adjacent chip positions in the template signal. From these points we arrive at the following conclusions,

1) Any pulse of the interferer within the $(k-1)^{th}$ bit duration can contribute to a correlation equal to $R_{wb}(\tau)$, with the probability $(1/N_h)$.

2) Within the k^{th} bit's region, all the pulse origins can have an additional shift equal to $\delta, 0$ or $-\delta$; depending on the dibit $D_{k-1}D_k$. With respect to the desired user's template pulses falling in this region, the distance to the closest pulse origin can take three different values; τ when $D_{k-1}D_k$ is 00 or 11 , μ^+ when $D_{k-1}D_k$ is 01 and μ^- when $D_{k-1}D_k$ is 10, where

$$\mu^+ = \begin{cases} \tau+\delta & ; if\ \tau+\delta \le \dfrac{T_c}{2} \\ \\ \tau+\delta-T_c & ; if\ \tau+\delta \ge \dfrac{T_c}{2} \end{cases}, \tag{3.4}$$

$$\mu^- = \begin{cases} \tau-\delta & ; if\ \tau-\delta \ge -\dfrac{T_c}{2} \\ \\ T_c+\tau-\delta & ; if\ \tau-\delta \le -\dfrac{T_c}{2} \end{cases}. \tag{3.5}$$

And the corresponding interference term is $R_{wb}(\tau)$ or $R_{wb}(\mu^+)$ or $R_{wb}(\mu^-)$. We infer from the above conclusions that, for a given τ, the total interference from the interfering signal can only assume the following values:

$$I^u_{PPM/\tau} = \begin{cases} [n_1 R_{wb}(\tau) + n_2 R_{wb}(\mu^+)] \\ or \\ [n_1 R_{wb}(\tau) + n_2 R_{wb}(\mu^-)] \end{cases} \tag{3.6}$$

where n_1 and n_2 are integers with, $n_1 \le N_s$, $n_2 \le N_s$ and $n_1 + n_2 \le N_s$. This clearly shows that the interferences caused by individual pulses in different frames are

not purely independent which contradicts with the assumptions in [32-34], [37]. By evaluating the corresponding probabilities of the discrete values of $I^u_{PPM/\tau}$ and using the distribution of τ, the statistical modeling of I^u_{PPM} is complete.

With respect to the possible values of $I^u_{PPM/\tau}$, which are given by (3.6), we define the following set of probabilities, $P_1(n_1, n_2)$ and $P_2(n_1, n_2)$.Where

$$P_1(n_1, n_2) = P(I^u_{PPM/\tau} = n_1 \times R_{wb}(\tau) + n_2 \times R_{wb}(\mu^+)) \tag{3.7}$$

$$P_2(n_1, n_2) = P(I^u_{PPM/\tau} = n_1 \times R_{wb}(\tau) + n_2 \times R_{wb}(\mu^-)). \tag{3.8}$$

$P_1(n_1, n_2)$ and $P_2(n_1, n_2)$ can be expressed as follows (refer to the proofs in section 3.2.5.1)

$$P_1(n_1, n_2) = P_2(n_1, n_2) = P_{01}(n_1, n_2) + P_{00}(n_1, n_2), \tag{3.9}$$

where $P_{00}(n_1, n_2) = P\left(\left[I^u_{PPM/\tau} = n_1 \times R_{wb}(\tau) + n_2 \times R_{wb}(\mu^+)\right] \Big/ D_{k-1}D_k = 00\right)$

and $P_{01}(n_1, n_2) = P\left(\left[I^u_{PPM/\tau} = n_1 \times R_{wb}(\tau) + n_2 \times R_{wb}(\mu^+)\right] \Big/ D_{k-1}D_k = 01\right)$.

3.2.3 TH-PAM System

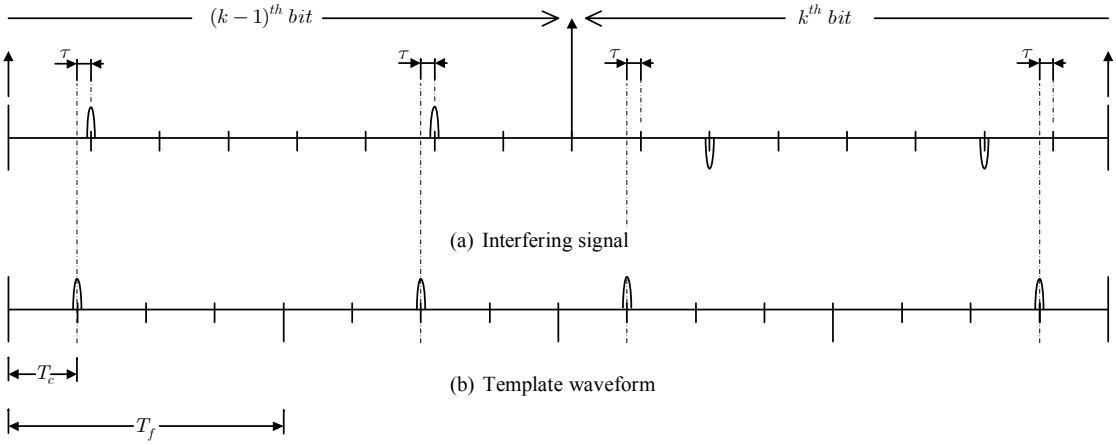

Fig. 3.3 An interfering signal (a) compared against the template waveform (b) of the desired user with $N_s = 4$ and $T_c = T_f / 4$ for TH-PAM system

Fig. 3.3 shows an interfering signal against the correlating template waveform for a TH-PAM system. According to the model described in section 3.2, the interference related to the first template pulse is $\pm R_{ww}(\tau)$, where the sign depends on the $(k-1)^{th}$ data bit, and the probability of this occurrence is $1/N_h$. Similarly all the template pulses (note that now the template pulse is a single mono-pulse) in the k^{th} bit duration can generate a correlation $\pm R_{ww}(\tau)$, with the probability $1/N_h$, and the sign is determined by the k^{th} bit.

Therefore, the total interference over the bit duration for a given τ becomes

$$I^u_{PAM/\tau} = n_1 R_{ww}(\tau), \tag{3.10}$$

where, $n_1 \in \left\{-N_s, -(N_s-1), ..., N_s\right\}$. The probability $P\left(I^u_{PAM/\tau} = n_1 R_{ww}(\tau)\right)$ is defined as $P(n_1)$, where

$$P(n_1) = P(-n_1) = P_{00}(n_1) + P_{01}(n_1) + P_{10}(n_1) \tag{3.11}$$

for $n_1 \in \{0, ..., N_s\}$ (refer to section 3.2.5.2 for the proofs), where

$P_{00}(n_1) = P\left(\left[I^u_{PAM/\tau} = n_1 R_{ww}(\tau)\right] / \; D_{k-1}D_k = 00\right)$,

$P_{01}(n_1) = P\left(\left[I^u_{PAM/\tau} = n_1 R_{ww}(\tau)\right] / \; D_{k-1}D_k = 01\right)$ and

$P_{10}(n_1) = P\left(\left[I^u_{PAM/\tau} = n_1 R_{ww}(\tau)\right] / \; D_{k-1}D_k = 10\right)$.

3.2.4 DS-PAM System

Fig. 3.4 shows a typical interfering condition of DS-PAM signals. Since the factor $(-1)^{D^u_i}$ and the chip code a^u_i are independent equiprobable bipolar random variables

and both jointly modify the pulse polarity, the resulting coefficient $(-1)^{D_i^u} \times a_i^u$ can be modeled by another equiprobable bipolar random variable.

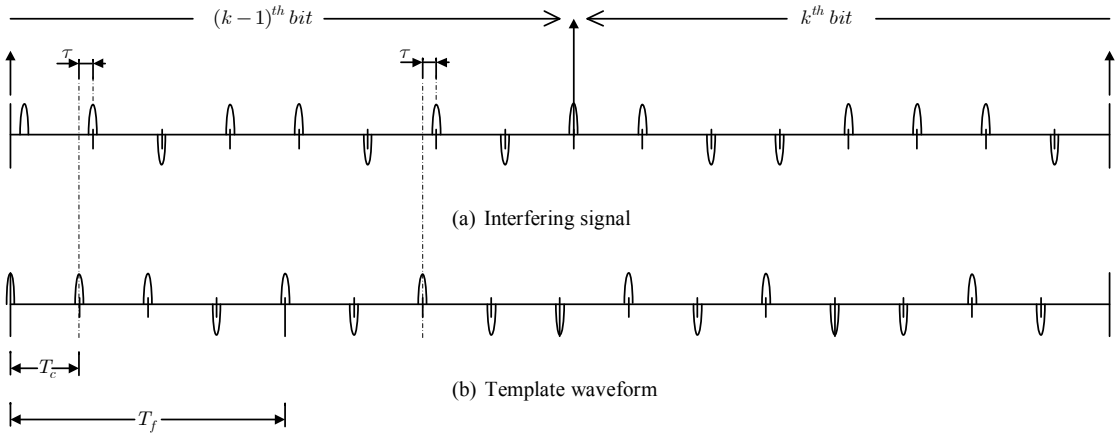

Fig. 3.4 An interfering signal (a) compared against the template waveform (b) of the desired user with $N_s = 16$ for a DS-PAM system.

Therefore, with the assumption of a long code, the need for considering the bit changeover is eliminated. Each template pulse will generate an interference component $\pm R_{ww}(\tau)$ with equal probability, and the possible values of the total interference conditioned on τ is given by

$$I^u_{DS-PAM/\tau} = n_1 R_{ww}(\tau), \tag{3.12}$$

where $n_1 \in \left\{-N_s, -N_s + 2, \ldots\ldots N_s - 2, N_s\right\}$. The conditional probability $P_{DS}(n_1)$ is defined by $P_{DS}(n_1) = P\left(I^u_{DS-PAM/\tau} = n_1 R_{ww}(\tau)\right)$.

3.2.5 Deriving the probability functions

In this section, the basic guidelines for deriving the probabilities are provided. Derivations are presented for TH-PPM, TH-PAM and DS-PAM. If the reader is interested in OOK modulation, the derivations for PAM can be used to infer the respective formulas as OOK is also a kind of amplitude modulation.

3.2.5.1 TH-PPM

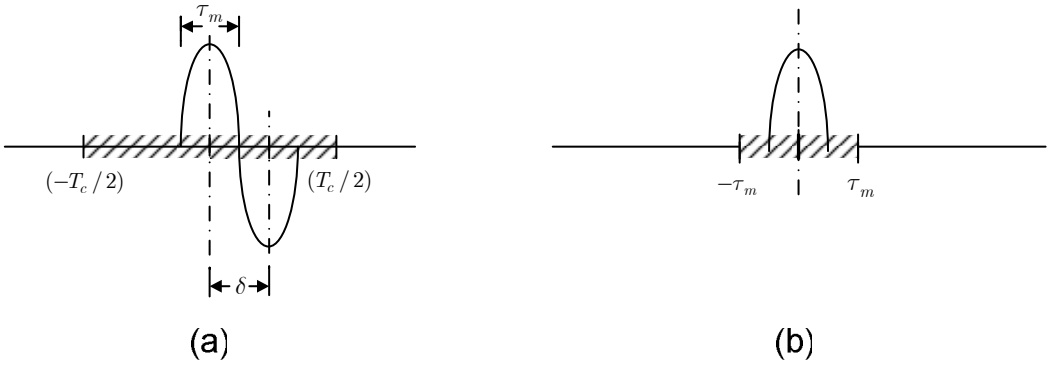

Fig. 3.5 (a) The first template pulse in the template waveform for PPM (enlarged). (b) The first template pulse in the template waveform of PAM signal (enlarged).

Fig. 3.5(a) is an enlarged version of a single template pulse in the desired user's template signal. (here, we have selected the first template pulse without loss of generality). The range of τ is denoted by the shaded region. Due to the bit changeover, the template pulses in the desired user signal are divided in to two sets, each having $m_{(k-1)}$ and $m_{(k)}$ number of template pulses respectively, where $m_{(k-1)} + m_{(k)} = N_s$ (Fig 3.2). Since the position of bit changeover is a uniform random variable, each value that the pair $m_{(k-1)}, m_{(k)}$ can take has an average probability $1/N_s$. We will consider all the four possible dibit states separately.

A. Dibit state '00':

The related probabilities are denoted by $P_{00}(n_1, n_2)$. When this occurs $P_{00}(n_1, n_2) = 0; \forall n_2 \neq 0$. By considering all the possible combinations of n_1 interfering pulses, we obtain

$$P_{00}(n_1, 0) = \frac{1}{4} C_{n_1}^{N_s} (1/N_h)^{n_1} (1 - 1/N_h)^{N_s - n_1}. \tag{3.13}$$

B. Dibit state '01':

In this case the interference contribution from the $(k-1)^{th}$ bit and the $(k)^{th}$ bit are, $n_1 R_{wb}(\tau)$ and $n_2 R_{wb}(\mu^-)$, respectively. By considering the available combinations for all the possible bit change-over positions we obtain

$$P_{01}(n_1,n_2) = \frac{1}{4}\sum_{j=(n_1-1)}^{(N_s-n_2-1)} \frac{1}{N_s} C_{n_1}^{(j+1)} (1/N_h)^{n_1} (1-1/N_h)^{(j-n_1+1)} \cdot C_{n_2}^{(N_s-j-1)} (1/N_h)^{n_2} (1-1/N_h)^{(N_s-j-n_2-1)} \quad . \quad (3.14)$$

C. Dibit states '10' and '11':

The corresponding probabilities are defined by, $P_{10}(n_1,n_2)$ and $P_{11}(n_1,n_2)$. By noting the similarity of these two cases with previous two cases we obtain,

$$P_{10}(n_1,n_2) = P_{01}(n_1,n_2), \quad (3.15)$$

and

$$P_{11}(n_1,n_2) = P_{00}(n_1,n_2). \quad (3.16)$$

3.2.5.2 TH-PAM

The methodology is similar to that explained in 3.2.5.1. Fig. 3.5 (b) is an enlarged version of a single template pulse in the desired user's template signal. Now we consider the possible dibit combinations referring to Fig. 3.3.

A. Dibit state '00':

In this case $n_1 \in \{0,1,.....N_s\}$, and by considering all the possible combinations $P_{00}(n_1)$ can be written as

$$P_{00}(n_1) = \tfrac{1}{4} C_{n_1}^{N_s} (1/N_h)^{n_1} (1 - 1/N_h)^{N_s - n_1} . \tag{3.17}$$

B. Dibit state '01':

In this case $n_1 \in \{-N_s.....N_s\}$, and the corresponding probability is given by

$$P_{01}(n_1) = \tfrac{1}{4} \sum_{j=|n_1|-1}^{N_s-1} \tfrac{1}{N_s} \sum_{r=|n_1|}^{\min(N_s-j+r-1,\, j)} C_r^{j+1} \left(1/N_h\right)^r \left(1 - 1/N_h\right)^{j+1-r} C_{r-|n_1|}^{N_s-j-1} \left(1/N_h\right)^{r-|n_1|} \left(1 - 1/N_h\right)^{N_s+|n_1|-j-r-1} \tag{3.18}$$

C. Dibit states '10' and '11':

The probabilities for the dibit states '10' and '11' are respectively denoted by $P_{10}(n_1)$ and $P_{11}(n_1)$. By using the symmetry we get

$$P_{10}(n_1) = P_{01}(-n_1), \tag{3.19}$$

for $n_1 \in \{-N_s.....N_s\}$, and

$$P_{11}(n_1) = P_{00}(-n_1), \tag{3.20}$$

for $n_1 \in \{0,-1,..... - N_s\}$.

3.2.5.3 DS-PAM

First we will consider the case where $n_1 > 0$. The resulting total interference will be equal to $n_1 R_{ww}(\tau)$ if exactly $(N_s + n_1)/2$ pulses in the interfering signal (Fig. 3.4) have the same polarity as the corresponding template pulses (note that $(N_s + n_1)/2$ is an integer value). Therefore $P_{DS}(n_1)$ is the probability that exactly $(N_s + n_1)/2$ pulses will have the same polarity. From the details in section 3.2.4, it is obvious that the probability that a pulse has same or opposite polarity as its closest template pulse is $1/2$. Therefore, it is straight forward to show using binomial

distribution theory that the probability for this event is $C_{\frac{(N_s+n_1)}{2}}^{N_s}(1/2)^{\frac{(N_s+n_1)}{2}} \times (1/2)^{\frac{(N_s-n_1)}{2}}$; i.e. $P_{DS}(n_1) = C_{\frac{(N_s+n_1)}{2}}^{N_s}(1/2)^{N_s}$ for $n_1 > 0$.

Since $P_{DS}(n_1)$ is even symmetric we obtain

$$P_{DS}(n_1) = C_{\frac{(N_s+|n_1|)}{2}}^{N_s}(1/2)^{N_s}\ , \tag{3.21}$$

for $n_1 \in \{-N_s, -N_s+2, \ldots\ldots N_s-2, N_s\}$.

3.3 Derivation of CF and BER in AWGN channels

The modeling of the interference contributed by a single user is presented in section 3.2 These results can now be applied to evaluate the system performance, in an additive white Gaussian noise (AWGN) channel. We choose to follow the decision variable-CF approach [39] to derive the bit error rates.

3.3.1 TH- PPM

Considering an AWGN channel, the total MAI component I_{PPM} is now given by,

$$I_{PPM} = \sum_{u=1}^{N_u-1} I_{PPM}^{u}\ . \tag{3.22}$$

By definition, the CF of I_{PPM} is given by

$$\Phi_{I_{PPM}}(w) = E\{\exp(jwI_{PPM})\}. \tag{3.23}$$

And $\Phi_{(I_{PPM}^{u})}(w)$ can be expressed as

$$\Phi_{(I_{PPM}^{u})}(w) = \frac{1}{T_c}\int_{\frac{-T_c}{2}}^{\frac{T_c}{2}} \Phi_{(I_{PPM/\tau}^{u})} d\tau\ , \tag{3.24}$$

where the conditional CF $\Phi_{(I^u_{PPM}/\tau)}$ is given by

$$\Phi_{(I^u_{PPM}/\tau)} = \sum_{n_1=0}^{Ns}\sum_{n_2=0}^{Ns-n_1} P_1(n_1,n_2)\exp\big(jw\big(n_1R_{wb}(\tau)+n_2R_{wb}(\mu^+)\big)\big) + \sum_{n_1=0}^{Ns}\sum_{n_2=0}^{Ns-n_1} P_2(n_1,n_2)\exp\big(jw\big(n_1R_{wb}(\tau)+n_2R_{wb}(\mu^-)\big)\big) \tag{3.25}$$

Generally, the pulse waveform $w(t)$ assumes a symmetric shape; therefore the distribution of I^u_{PPM} also becomes symmetric. If the modulation is orthogonal, the distribution of I^u_{PPM} can be symmetric even if the pulse shape is not symmetric. Hence, we can write

$$\begin{aligned}\Phi_{(I^u_{PPM})}(w) &= \Phi_{(-I^u_{PPM})}(w)\\ &= \frac{1}{2}\big(\Phi_{(I^u_{PPM})}(w)+\Phi_{(-I^u_{PPM})}(w)\big)\end{aligned} \tag{3.26}$$

By applying (3.26), we get the following real valued expressions for $\Phi_{(I^u_{PPM})}(w)$,

$$\Phi_{(I^u_{PPM})}(w) = \frac{1}{T_c}\int_{\frac{-T_c}{2}}^{\frac{T_c}{2}}\Phi' d\tau \tag{3.27}$$

where

$$\Phi' = \sum_{n_1=0}^{Ns}\sum_{n_2=0}^{Ns-n_1} P_1(n_1,n_2)\cos\big[w\big(n_1R_{wb}(\tau)+n_2R_{wb}(\mu^+)\big)\big] + \sum_{n_1=0}^{Ns}\sum_{n_2=0}^{Ns-n_1} P_2(n_1,n_2)\cos\big[w\big(n_1R_{wb}(\tau)+n_2R_{wb}(\mu^-)\big)\big] \tag{3.28}$$

If I^u_{PPM} is not symmetric, (3.24) should be used in its complex form. Since I^u_{PPM} are assumed to be independent and identical to each other, $\Phi_{I_{PPM}}(w)$ is given by

$$\Phi_{I_{PPM}}(w) = \left[\Phi_{I^{u}_{PPM}}(w)\right]^{N_u - 1}. \tag{3.29}$$

The CF of the AWGN component n_{PPM} is given by

$$\Phi_{n_{PPM}}(w) = \exp\left(\frac{-w^2 N_o R_{wb}(0) N_s}{2}\right), \tag{3.30}$$

where N_o is the power spectral density of the noise.

Now the bit error probability of the binary modulation scheme is given by

$$\begin{aligned} P_e &= \tfrac{1}{2} P(r \geq 0 / D_j = 1) + \tfrac{1}{2} P(r \leq 0 / D_j = 0) \\ &= P(r \leq 0 / D_j = 0) \\ &= P(I_{PPM} + n_{ppm} \leq -N_s \sqrt{E} R_{wb}(0) / D_j = 0). \end{aligned} \tag{3.31}$$

With the help of few Fourier transform manipulations, P_e can be expressed in the following form

$$P_e = \frac{1}{2} - \frac{1}{2\pi} \int_{-\infty}^{\infty} \frac{\Phi_{I_{PPM}}(-w)}{jw} \Phi_{n_{PPM}}(w) \exp\left(jw\sqrt{E} N_s R_{wb}(0) \right) dw. \tag{3.32}$$

Since $\Phi_{I_{PPM}}(w)$ and $\Phi_{n_{PPM}}(w)$ are real and even-symmetric, the integral in equation (3.32) reduces to a convenient real function form as

$$P_e = \frac{1}{2} - \frac{\sqrt{E} N_s R_{wb}(0)}{\pi} \int_{0}^{\infty} \Phi_{I_{PPM}}(w) \Phi_{n_{PPM}}(w) \operatorname{sinc}\left(\frac{\sqrt{E} N_s R_{wb}(0) w}{\pi} \right) dw. \tag{3.33}$$

With the substitutions $w_o = \sqrt{E} w$ and $\gamma = \dfrac{N_s E}{N_o}$, equation (3.33) takes an alternative form

$$P_e = \frac{1}{2} - \frac{N_s R_{wb}(0)}{\pi} \int_{0}^{\infty} \Phi_{\bar{I}_{PPM}}(w_o) \exp\left(\frac{-w_o^2 N_s^2 R_{wb}(0)}{2\gamma} \right) \operatorname{sinc}\left(\frac{N_s R_{wb}(0) w_o}{\pi} \right) dw_o, \tag{3.34}$$

where $\Phi_{\bar{I}_{PPM}}(w_o)$ is the CF of the normalized interference and is given by

$$\Phi_{\bar{I}_{PPM}}(w_o) = E\left\{\exp\left[jw_o\left(\frac{I_{PPM}}{\sqrt{E}}\right)\right]\right\}. \tag{3.35}$$

3.3.2 TH-PAM

Similarly the CF of the total interference I_{PAM} is given by

$$\Phi_{I_{PAM}}(w) = \left[\Phi_{I^u_{PAM}}(w)\right]^{N_u-1}, \tag{3.36}$$

where

$$\Phi_{(I^u_{PAM})}(w) = \frac{1}{T_c}\int_{-\tau_m}^{\tau_m}\Phi_{(I^u_{PAM/\tau})}d\tau + P_o. \tag{3.37}$$

And the conditional CF $\Phi_{(I^u_{PAM/\tau})}$ is given by

$$\Phi_{(I^u_{PAM/\tau})} = 2\sum_{0}^{Ns}P(n_1)\times\cos(wn_1R_{ww}(\tau)). \tag{3.38}$$

The constant term P_o in (3.37) represents the probability that τ falls within $\left[-\frac{T_c}{2},-\tau_m\right]\bigcup\left[\tau_m,\frac{T_c}{2}\right]$, i.e the probability that $R_{ww}(\tau)$ is strictly zero within $\left[-\frac{T_c}{2},\frac{T_c}{2}\right]$. Therefore, $P_0 = 1-\frac{2\tau_m}{Tc}$(the condition $2\tau_m \le T_c$ is clearly understood in UWB signal design). In analogy with (3.31) we can obtain the following probability of error for a PAM system

$$P_e = P(I_{PAM} + n_{PAM} \le -N_s\sqrt{E}R_{ww}(0)/D_j = 0). \tag{3.39}$$

And,

$$\Phi_{n_{PAM}}(w) = \exp\left(\frac{-w_o^2N_s^2R_{ww}(0)}{4\gamma}\right). \tag{3.40}$$

It can be noted that, the PDF of I_{PAM} is symmetric regardless of the pulse shape. Using the symmetry of I_{PAM}, the BER of a binary PAM system is given by

$$P_e = \frac{1}{2} - \frac{N_s R_{ww}(0)}{\pi} \int_0^{\infty} \Phi_{\bar{I}_{PAM}}(w_o) \exp\left(\frac{-w_o^2 N_s^2 R_{ww}(0)}{4\gamma}\right) \operatorname{sinc}\left(\frac{N_s R_{ww}(0) w_o}{\pi}\right) dw_o , \tag{3.41}$$

where $\bar{I}_{PAM}$ has similar definition as (3.35).

3.3.3 DS-PAM

The conditional CF of the interference from a user in DS-PAM systems is given by

$$\Phi_{(I^u_{DS-PAM/\tau})} = \sum_{n_1 \in \{-N_s, -N_s+2, \ldots, N_s\}} P_{DS}(n_1) \times \exp(jwn_1 R_{ww}(\tau)) . \tag{3.42}$$

Hence, $\Phi_{(I^u_{DS-PAM})}$ is given by $\Phi_{(I^u_{DS-PAM})} = \frac{1}{T_c} \int_{-\tau_m}^{\tau_m} \Phi_{(I^u_{DS-PAM/\tau})} d\tau + P_o$, where $P_o = 1 - \frac{2\tau_m}{T_c}$ is the probability that τ falls out side the range $\left[-\tau_m, \tau_m\right]$; i.e the probability that $I^u_{DS-PAM/\tau}$ is strictly zero.

Equation (3.42) can be reduced to a real function form by using the symmetry of n_1, hence we obtain

$$\Phi_{(I^u_{DS-PAM})} = \frac{2}{T_c} \int_{-\tau_m}^{\tau_m} \sum_{n_1 \in \{N_s, N_s-2, \ldots, 0 \, or \, 1\}} P_{DS}(n_1) \times \cos(wn_1 R_{ww}(\tau)) d\tau + P_o . \tag{3.43}$$

It should be noted that the lower limit of the summation in (3.43) is either 0 or 1 depending on whether N_s is odd or even respectively. Finally the average bit error probability for DS-PAM systems is given by

$$P_e = \frac{1}{2} - \frac{N_s R_{ww}(0)}{\pi} \int_0^{\infty} \Phi_{\bar{I}_{DS-PAM}}(w_o) \exp\left(\frac{-w_o^2 N_s^2 R_{ww}(0)}{4\gamma} \right) \mathrm{sinc}\left(\frac{N_s R_{ww}(0) w_o}{\pi} \right) dw_o \,. \quad (3.44)$$

3.4 Numerical results

In this section we present some numerical examples, aiming to verify the theoretical BER formulas derived. The derivations are independent of pulse shapes and therefore, these results are applicable to any kind of pulse shapes. For simulation purposes the pulse waveform $w(t)$ used here is the second derivative of the Gaussian pulse, and is given by

$$w(t) = \left[1 - 16\pi \left(\frac{t}{\tau_m} \right)^2 \right] \exp\left(-8\pi \left(\frac{t}{\tau_m} \right)^2 \right). \quad (3.45)$$

The normalized autocorrelation corresponding to this pulse is given by [27],

$$R_{ww}(\tau) = \left[1 - 16\pi \left(\frac{t}{\tau_m} \right)^2 + \frac{64\pi^2}{3} \left(\frac{t}{\tau_m} \right)^4 \right] \exp\left(-4\pi \left(\frac{t}{\tau_m} \right)^2 \right). \quad (3.46)$$

The following system parameters are assumed unless stated otherwise. $N_u = 25$, $N_h = 12$, and $\tau_m = 0.5ns$. Theoretical and simulation results of TH-PPM systems are compared in Fig. 3.6 for an orthogonal PPM system and in Fig. 3.7 for a non-orthogonal PPM system. Two different values, 4 an 8, are considered for the spreading gain. Due to the shorter chip duration, the upward turning of the curve towards the error floor occurs at lower SNR values in Fig. 3.7 compared to that in Fig. 3.6.

Fig. 3.8 and Fig. 3.9 compare the performances of TH-PAM for widely and closely spaced chips, respectively. Fig. 3.10 presents comparison for the DS-PAM system

performance. In all the above cases the theoretical and simulation BER matches exactly. This validates our theoretical derivations. The simulations consider an AWGN channel with full asynchronism. The small deviations of the simulation curves from the theoretical curves are inevitable due to practical simulation inaccuracies which can be improved only by increasing the number of Monte-Carlo cycles.

In the theoretical evaluations, the BER is highly sensitive to the accuracy of the numerical integration at higher SNR values. There are two main factors contributing to the error in numerical integration, one is the density of the sampling points chosen and the other is the truncation error involved in evaluating the infinite integrals in (3.32), (3.33), (3.34), (3.41) and (3.44). More number of samples is needed and the truncation window should be large at high SNR values.

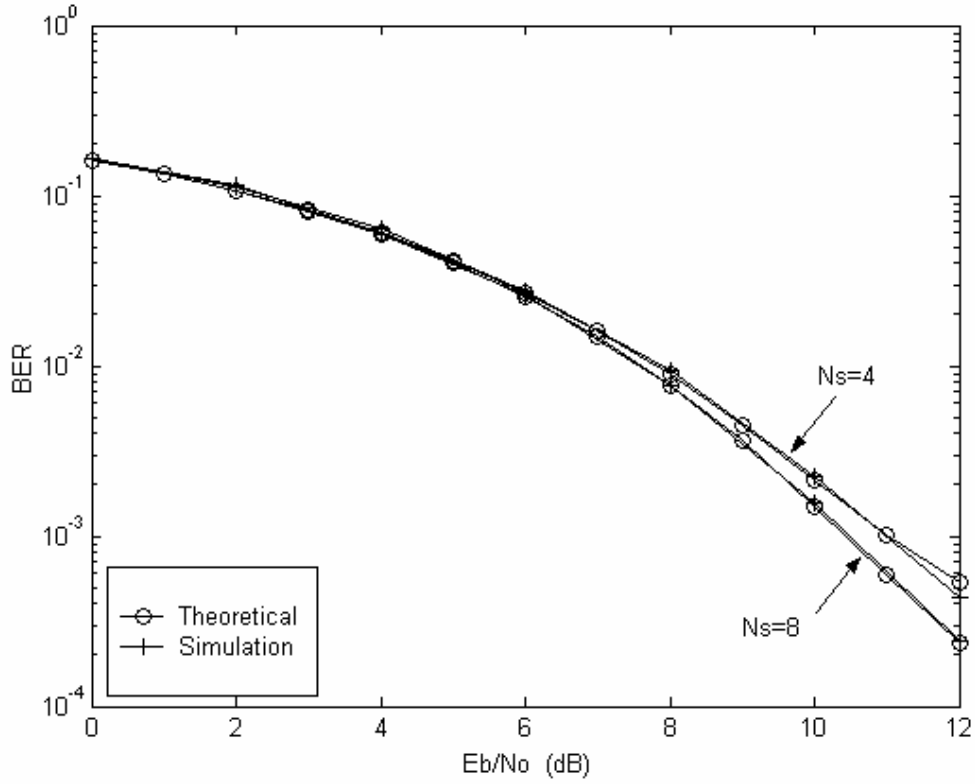

Fig. 3.6 Theoretical and simulation performance of TH-PPM compared for $N_s = 4$ and $N_s = 8$, with $T_c = 8ns$ and $\delta = 1.5ns$

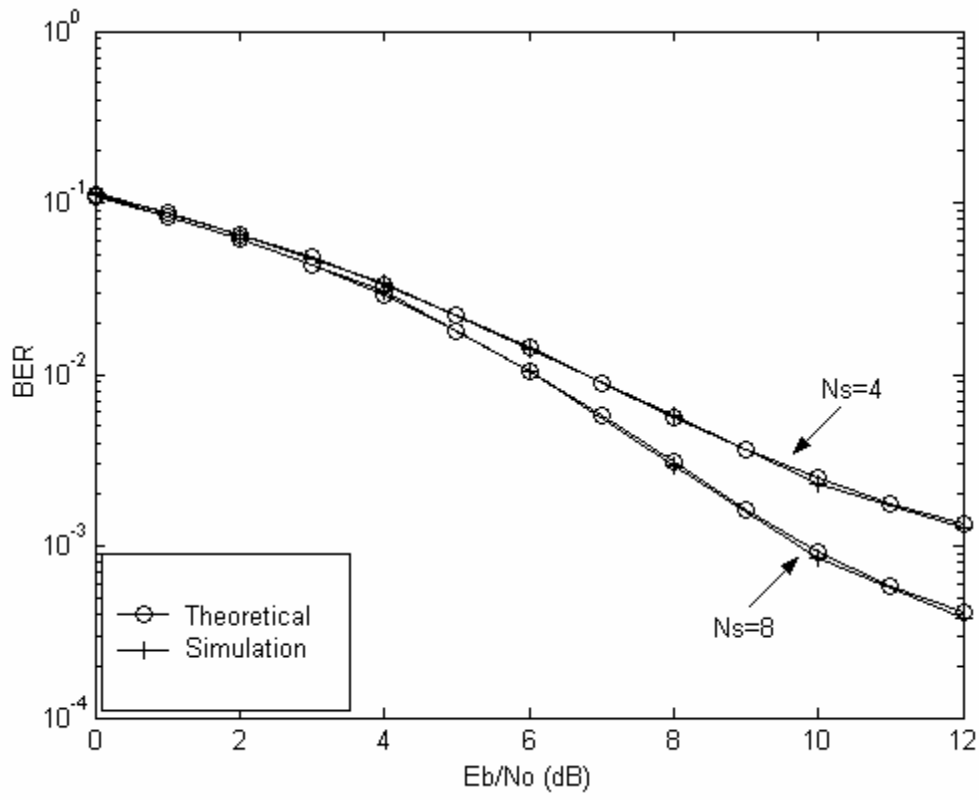

Fig. 3.7 Theoretical and simulation performance of TH-PPM compared for $N_s = 4$ and $N_s = 8$, with $T_c = 2ns$ and $\delta = 0.135ns$.

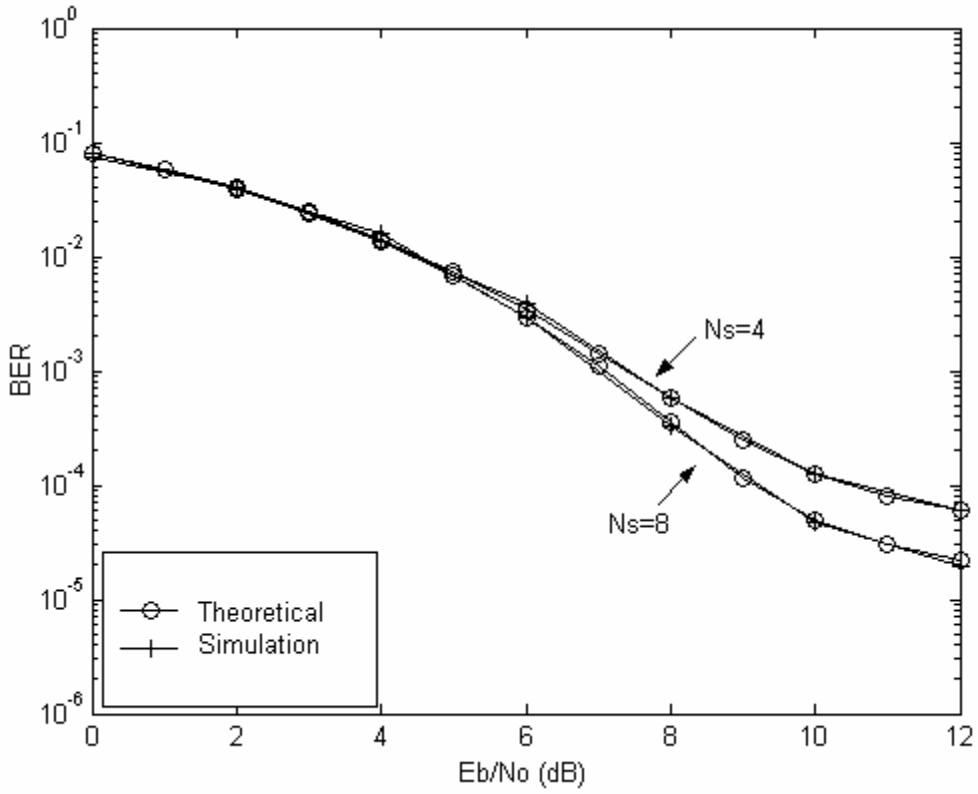

Fig. 3.8 Theoretical and simulation performance of TH-PAM compared for $N_s = 4$ and $N_s = 8$, with $T_c = 8ns$ (widely spaced chips).

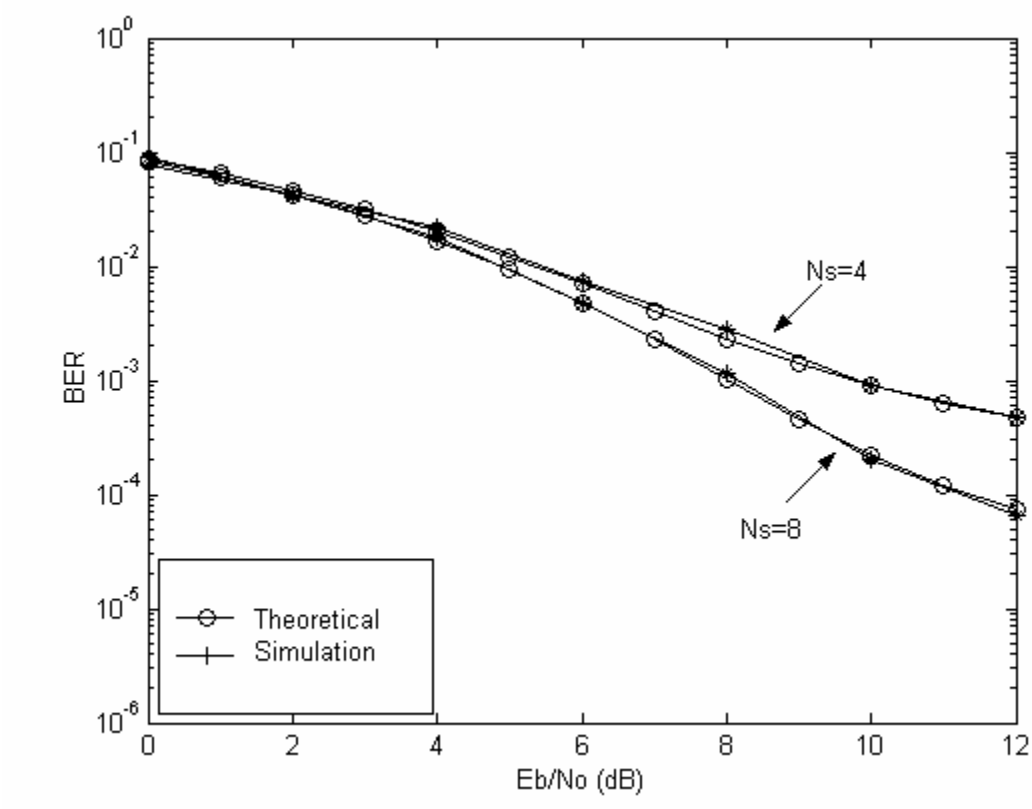

Fig. 3.9 Theoretical and simulation performance of TH-PAM compared for $N_s = 4$ and $N_s = 8$, with $T_c = 2ns$ (closely spaced chips).

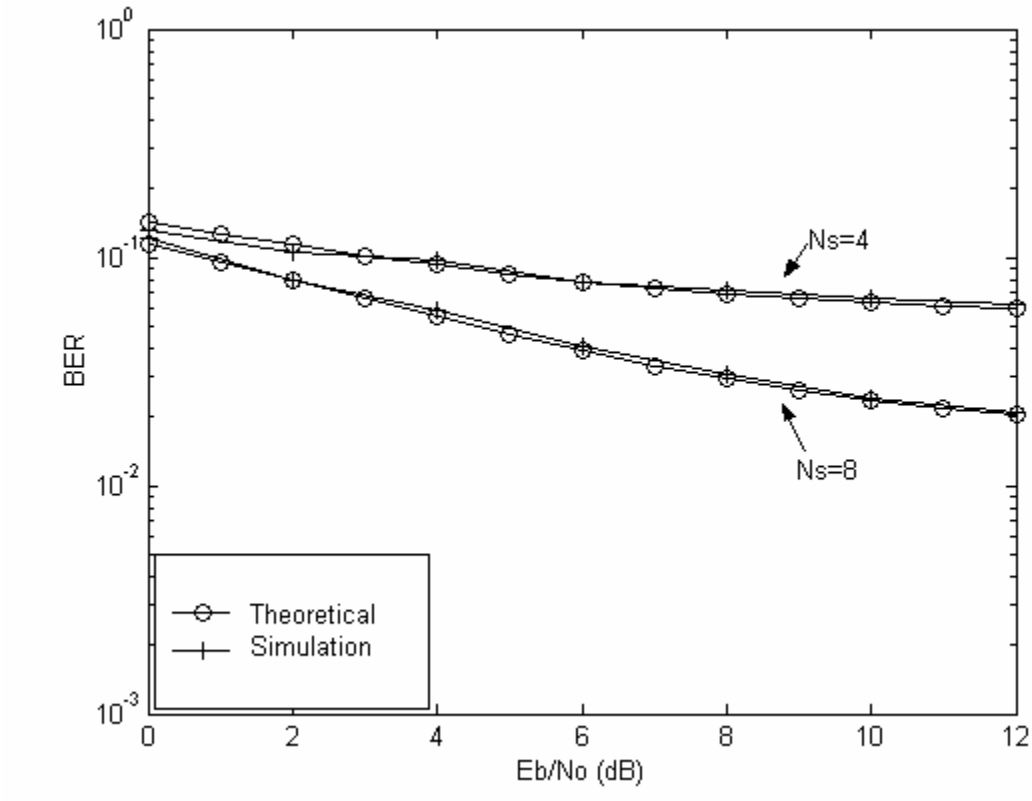

Fig. 3.10 Theoretical and simulation performance of DS-PAM compared for $N_s = 4$ and $N_s = 8$, with $T_c = 2ns$

3.5 Conclusions

In this chapter, the exact statistical models of the MAI in TH-PPM, TH-PAM and DS-PAM are derived for an AWGN channel. It is developed from basic principles using the geometric properties of the interfering signals. In contrast to the previously proposed methods, this method considers a fully asynchronous channel and proves that the interference components within each frame are not independent. This model is used to compute the CF of the total interference and hence derive the formulas for exact BER for binary UWB-IR systems. The BER formulas are verified by comparing the results with that of Monte-Carlo simulations, and the final outcome is that the theoretical derivations match exactly with the simulation results.

PERFORMANCE ANALYSIS IN FADING CHANNELS

In this chapter the performance of a correlator receiver in fading channel is derived. In addition, an accurate method to numerically evaluate the CF of a lognormal random variable is also presented.

4.1 Simplified channel model

It is a formidable task to develop accurate methods to find the BER performance using the channel model in section 2.2, because this model contains multiple clusters (of rays) with random cluster-starting times and a segmented power decaying profile (PDP). Furthermore, the channel gain is modeled as a log-normal random variable.

Therefore, in order to make the analysis theoretically tractable, certain simplifying assumptions are made. The channel gain $\left|h_l^u\right|$ is defined as a single lognormal variable, i.e $20\log_{10}\left(\left|h_l^u\right|\right) \sim N\left(\mu_l^u, \sigma_l^u\right)$. The PDP is defined by a simple decaying exponential function and it can be simply expressed in terms of the path number as $E\left\{(h_l^u)^2\right\} = e^{-\rho l}$, where ρ is the decay factor. Finally the arrival times are assumed to be fixed and evenly spaced (However, the derivations presented later are also valid for the case where the arrival times are unevenly spaced). A similar simplified model is used in [18].

4.2 CF based approach

The total interference of a user, I^u (either I_{PPM}^u or I_{PAM}^u or I_{DS-PAM}^u) is statistically defined for TH-PPM, TH-PAM and DS-PAM modulations in AWGN channel

conditions in the last chapter. In fading multipath channels, the basic element in modeling the multiple access interference is I_l^u, the interference caused by the l^{th} arrival path from the u^{th} user.

I_l^u can be modeled as a product of two random variables (R.V), i.e

$$I_l^u = h_l^u \times I(\tau), \tag{4.1}$$

where $I(\tau)$ is statistically equivalent to I^u, defined for TH-PPM, TH-PAM and DS-PAM under the AWGN channel conditions in the last chapter. And, τ has been defined previously. It should be noted that the path and user dependency of I_l^u is attributed to the gain parameter h_l^u. Further, $I(\tau)$ and h_l^u are assumed independent. This 'independent' assumption is reasonable since τ is defined as the distance to the closest chip position from the template pulse, whereas the distribution of h_l^u is determined by the absolute path arrival times as described in section 2.2.

The CF of I_l^u conditioned on $I(\tau)$ is defined by

$$\Phi_{I_l^u / I(\tau)}(w) = E\left\{ e^{jwI_l^u} / I(\tau) \right\}. \tag{4.2}$$

Therefore,

$$\Phi_{I_l^u}(w) = \int_{-\infty}^{\infty} \Phi_{I_l^u / I(\tau)}(w) \times P_{I(\tau)}(I)\, dI\,. \tag{4.3}$$

Since the statistics of $I(\tau)$ is already defined implicitly in section 3.2 for TH-PPM, TH-PAM and DS-PAM, (4.3) is solvable accurately if a closed form solution for $\Phi_{I_l^u / I(\tau)}(w)$ is known.

The channel coefficient h_l^u has a double sided lognormal distribution according to the channel model stated in [9]. Therefore, for a given value of $I(\tau)$, I_l^u can be

equivalently modeled by $p|I_l^u|$, where p represents the equi-probable positive and negative polarities and has the distribution

$$P_p(p) = 0.5\,(\,\delta(p+1) + \delta(p-1)\,)\,. \tag{4.4}$$

And the distribution of $\left|I_l^u{}_{/\,I(\tau)}\right|$ is also lognormal since it is generated by multiplying a lognormal variable by a constant. Therefore,

$$\begin{aligned}\Phi_{I_l^u\,/\,I(\tau)}(w) &= \int_{-\infty}^{\infty} P_{I_l^u\,/\,I(\tau)}(I_l^u)\exp(\,jwI_l^u\,)\,dI_l^u \\ &= \int_{0}^{\infty} P_{|I_l^u|\,/\,I(\tau)}(|I_l^u|)\cos(jw|I_l^u|)\,d|I_l^u|\ , \\ &= \mathrm{Re}\{\Phi_{LN}(w,\sigma,\mu)\}\end{aligned} \tag{4.5}$$

where, Φ_{LN} denotes the characteristic function of a log normal variable and $\mathrm{Re}(.)$ denotes the real part of an expression. The parameters σ and μ are given by

$$\sigma^2 = Var\left\{20\log_{10}\left(\left|I_l^u{}_{/\,I(\tau)}\right|\right)\right\}, \tag{4.6}$$

$$\mu = E\left\{20\log_{10}\left(\left|I_l^u{}_{/\,I(\tau)}\right|\right)\right\}. \tag{4.7}$$

But a simple closed form solution for the CF of a log normal variable is not known [40-41]. A solution is proposed in [42] in the form of an infinite series, but the evaluation of the series coefficients up to an order to achieve acceptable accuracy, is much difficult. Therefore the CF should be estimated by suitable numerical methods. Gaussian Quadrature methods are preferable as the integral can be approximated in the form of a finite series. A Gauss-Hemite quadrature integral is used in [43], but when tested for few sets of values of σ, μ and w, it was found that the method dose not work well over the possible ranges of values of the parameters. And in some cases the estimation errors are very high. A more detailed analysis is presented in [41] on the

numerical evaluation of the CF, where a method based on Cleanshaw-Curtis algorithm is proposed.

The particular problem addressed here requires the estimation of the CF over a larger range of μ. The parameter σ is a constant for a channel and its typical values are within 3dB to 6dB. It was found by our tests that a single approximation method is likely to fail over some sub ranges of μ values. Therefore in order to alleviate this, a multi-segmented approach is introduced.

The power of the l^{th} path can be related to $E\left\{(h_0^u)^2\right\}$, the power of the first path, by

$$E\left\{(h_l^u)^2\right\} = E\left\{(h_0^u)^2\right\} \times e^{-\rho l} \tag{4.8}$$

where $0 \le l \le (L-1)$, and ρ is the decay factor. Equally spaced paths are assumed in the theoretical model for convenience. The distribution of $|h_l^u|$ is given by

$$P_{|h_l^u|}(h) = \frac{20}{\ln(10)} \frac{1}{h} \frac{1}{\sqrt{2\pi}\sigma_1} \exp\left(\frac{-(20\log_{10}(h)-\mu_l^u)^2}{2\sigma_1^2}\right) \tag{4.9}$$

where σ_1 is the dB spread of the log normal fading i.e ($\ln(.)$ is the natural logarithm)

$$\sigma_1^2 = E\left\{(20\log_{10}(|h_l^u|) - \mu_l^u)^2\right\} \tag{4.10}$$

and μ_l^u can be written as

$$\mu_l^u = \mu_o^u - \frac{10}{\ln 10}\rho l\,. \tag{4.11}$$

Further, it is assumed that the parameters are independent of u. This assumption is quite valid in case of a centralized network with perfect power control, but it is deemed only to simplify the derivations otherwise. Therefore, the absolute values of all the

channel coefficients $h_o^u,...,h_{L-1}^u$ have equal dB spread σ_1 and different μ_l^u according to (4.11).

4.3 A Multi-segmented numerical approach for the evaluation of characteristic function

The function $\mathrm{Re}\{\Phi_{LN}(w,\sigma,\mu)\}$ is to be approximated over the possible ranges of values of σ and μ. σ remains constant for a particular channel. Parameter μ, which is given by the equation

$$\mu = \mu_l^u + 20\log_{10}(|I(\tau)|)\,. \tag{4.12}$$

spans over an infinite range $\left[-\infty,\ \mu_{_H}\right]$, where

$$\mu_{_H} = 20\log_{10}(|I(\tau)|_{\max}) + \mu_l^u \tag{4.13}$$

is a finite number. The value of $\mu_{_H}$ is controllable by scaling the total received signal, if required. With the help of a dummy variable x, $\mathrm{Re}\{\Phi_{LN}(w,\sigma,\mu)\}$ is expressed as

$$\mathrm{Re}\{\Phi_{LN}(w,\sigma,\mu)\} = \int_0^\infty \frac{20}{\ln 10}\frac{1}{x}\frac{1}{\sqrt{2\pi}\sigma}\exp\left(\frac{-(20\log_{10}(x)-\mu)^2}{2\sigma^2}\right)\times\cos(wx)\,dx\,. \tag{4.14}$$

An alternative form of (4.14), with the substitution $y = 20\log_{10}(x)$ is given by

$$\mathrm{Re}\{\Phi_{LN}(w,\sigma,\mu)\} = \int_{-\infty}^\infty \frac{1}{\sqrt{2\pi}\sigma}\exp\left(\frac{-(y-\mu)^2}{2\sigma^2}\right)\times\cos(w\times 10^{(y/20)})\,dy \tag{4.15}$$

By examining different Gaussian Quadrature methods, it was found that Gauss-Laguerre [44, 45] method provides good approximation for fairly large values of μ using (4.14). Therefore it is straight forward to show that

$$\mathrm{Re}\{\Phi_{LN}(w,\sigma,\mu)\} = \sum_{k=1}^{N_p} W(x_k) e^{x_k} \frac{20}{\ln 10} \frac{1}{x_k} \frac{1}{\sqrt{2\pi}\sigma} \times \exp\left(\frac{-(20\log_{10}(x_k)-\mu)^2}{2\sigma^2}\right) \times \cos(wx_k) \tag{4.16}$$

where x_k is the k^{th} zero of the ${N_P}^{th}$ order Laguerre polynomial L_{N_P}, and the corresponding weights $W(x_k)$ are given by

$$W(x_k) = \frac{x_k}{(N_p+1)^2 \left[L_{N_p+1}(x_k)\right]^2} \tag{4.17}$$

The integrand in (4.14) becomes a steeper function when μ grows smaller and because of this, the Gauss-Laguerre method becomes inaccurate even when N_p is set at a larger value (e.g. N_p = 32).

The alternative form (4.15) will help to resolve this problem since the integrand in (4.15) is a smooth function at all the values of y, except at the fast oscillating positive tail. For larger negative values of μ, the integrand can be truncated effectively within the range $[\mu - 5\sigma,\ \mu + 5\sigma\ ]$. The error in neglecting the tails is lower than $Q(5)$ $(\simeq 2.8\times10^{-7})$, where Q denotes the Gaussian Q-function (tail probability function). Therefore the truncated integral of $\mathrm{Re}\{\Phi_{LN}(w,\sigma,\mu)\}$ can be expressed as

$$\mathrm{Re}\{\Phi_{LN}(w,\sigma,\mu)\} \simeq \int_{\mu-5\sigma}^{\mu+5\sigma} \frac{1}{\sqrt{2\pi}\sigma} \exp\left(\frac{-(y-\mu)^2}{2\sigma^2}\right) \times \cos\left(w \times 10^{(y/20)}\right) dy \,. \tag{4.18}$$

This can be effectively computed by Gauss-Legendre integration [44, 45], which yields

$$\mathrm{Re}\{\Phi_{LN}(w,\sigma,\mu)\} \simeq 5\sigma \sum_{k=1}^{N_p} W(y_k) \frac{1}{\sqrt{2\pi}\sigma} \exp\left(\frac{-25{y_k}^2}{2}\right) \times \cos\left(w \times 10^{((5\sigma\, y_k+\mu)/20)}\right) \tag{4.19}$$

where y_k are the abscissas of the N_p^{th} order Legendre polynomial $G_{N_p}(y)$. And the weight factors $W(y_k)$ are given by

$$W(y_k) = \frac{2}{\left(1-y_k^2\right)\left[G'_{N_p}(y_k)\right]^2}, \tag{4.20}$$

where $G'_{N_p}(.)$ denotes the first order derivative of $G_{N_p}(.)$

Finally, by noting the fact that

$$\lim_{\mu\to-\infty}\left\{\frac{20}{\ln 10}\frac{1}{x}\frac{1}{\sqrt{2\pi}\sigma}\exp\left(\frac{-(20\log_{10}(x)-\mu)^2}{2\sigma^2}\right)\right\} = \delta(x) \tag{4.21}$$

where $\delta(.)$ is the Dirac delta function, the PDF is approximated by a delta function for extremely smaller values of μ which actually represents the condition of near zero interference.

4.4 CF of the Total Interference

From (4.3) and the results from chapter 3 (eq. 3.25, 3.38 and 3.42) we can derive $\Phi_{I_l^u}(w)$, under the fading channel condition, for all the UWB schemes considered in this thesis.

For TH-PPM, it is given by

$$\begin{aligned}\Phi_{I_l^u}(w) = \frac{1}{T_c}\int_{-\frac{T_c}{2}}^{\frac{T_c}{2}}\sum_{n_1=0}^{Ns}\sum_{n_2=0}^{Ns-n_1}\mathrm{Re}\left\{\Phi_{LN}(w,\sigma_1,\mu_1)\right\}P_1(n_1,n_2)\\ +\sum_{n_1=0}^{Ns}\sum_{n_2=0}^{Ns-n_1}\mathrm{Re}\left\{\Phi_{LN}(w,\sigma_1,\mu_2)\right\}P_2(n_1,n_2)d\tau\end{aligned} \tag{4.22}$$

where

$$\mu_1 = \mu_l^u + 20\log_{10}\left(\left|\left(n_1R_{wb}(\tau)+n_2R_{wb}(\mu^+)\right)\right|\right), \tag{4.23}$$

$$\mu_2 = \mu_l^u + 20\log_{10}\left(\left|\left(n_1R_{wb}(\tau)+n_2R_{wb}(\mu^-)\right)\right|\right). \tag{4.24}$$

For PAM, it is given by

$$\Phi_{I_l^u}(w) = \frac{1}{T_c}\int_{-\tau_m}^{\tau_m}\sum_{n_1=0}^{Ns} \mathrm{Re}\{\Phi_{LN}(w,\sigma_1,\mu_1)\}\,P_1(n_1)\,d\tau + P_o \tag{4.25}$$

where $\mu_1 = \mu_l^u + 20\log_{10}(|n_1 R_{ww}(\tau)|)$. And, for DS-PAM, it is given by

$$\Phi_{I_l^u}(w) = \frac{1}{T_c}\int_{-\tau_m}^{\tau_m}\sum_{n_1\,\in\,\{-N_s,-N_s+2,\ldots,N_s\}}^{Ns} \mathrm{Re}\{\Phi_{LN}(w,\sigma,\mu_1)\}\,P(n_1)\,d\tau + P_o \tag{4.26}$$

where $\mu_1 = \mu_l^u + 20\log_{10}(|n_1 R_{ww}(\tau)|)$.

It should be noted that once $\Phi_{I_o^u}$ is found, $\Phi_{I_l^u}$ can be estimated using the relationship

$$\Phi_{I_l^u}(w) = \Phi_{I_o^u}(w\sqrt{e^{-\rho l}}) \tag{4.27}$$

for $l \in \{1,2,.....L-1\}$.

To make the analysis tractable, it is also assumed that I_l^u are independent for $l \in \{0,1,2,.....L-1\}$, and as in the AWGN case the total interference from each user is assumed identical and independent. Therefore the CF of the total interference can be approximately given by,

$$\Phi_I(w) = \left[\prod_{l=0}^{L-1}\Phi_{I_o^u}(w\sqrt{e^{-\rho l}})\right]^{Nu}. \tag{4.28}$$

4.5 The BER probabilities of a correlator receiver

We consider that the first path, which is most probably the largest, is extracted at the receiver for detection. The conditional BER of TH-PPM system is given by

$$P_{e/h_o^u} = \frac{1}{2} - \frac{\sqrt{E}N_s R_{wb}(0)h_o^u}{\pi}\int_0^\infty \Phi_I(w)\exp\left(\frac{-Ew^2N_s^2R_{wb}(0)}{2\gamma}\right)\mathrm{sinc}\left(\frac{\sqrt{E}N_s R_{wb}(0)h_o^u w}{\pi}\right)dw$$

.(4.29)

Similarly, the conditional BER of TH- PAM and DS-PAM is given by

$$P_{e/h_o^u} = \frac{1}{2} - \frac{\sqrt{E}N_s R_{ww}(0)h_o^u}{\pi}\int_0^\infty \Phi_I(w)\exp\left(\frac{-Ew^2N_s^2R_{ww}(0)}{4\gamma}\right)\mathrm{sinc}\left(\frac{\sqrt{E}N_s R_{ww}(0)h_o^u w}{\pi}\right)dw$$

. (4.30)

The average BER is obtained by averaging P_{e/h_o^u} over h_o^u, and is given by

$$P_e = \int_{-\infty}^{\infty} P_{e/h_o^u} P_{h_o^u}(h_o^u)\,dh_o^u. \tag{4.31}$$

4.6 Numerical results

To verify the equations for fading channels the following parameters are used in conjunction with the channel model prescribed in Section 4.1. $\sigma = 6$ dB, $\mu_o^u = -1.3$, $\rho = 0.1408$ and $L = 10$. The theoretical performance curves presented for all the 3 systems agree well with the simulation curves (Fig. 4.1). But we cannot expect an exact match between them since the theoretical curves are obtained through an approximate method.

As explained in Section 4.3, three different methods are used; Gauss-Laguerre, Guass-Legendre and Dirac delta function, to accurately evaluate the CF over the possible ranges of values of μ. However, the segmentation of the range of μ does not have any clearly defined boundaries. These boundary values should be determined adaptively, for each situation, to minimize the estimation error, and are dependant on the value of σ .

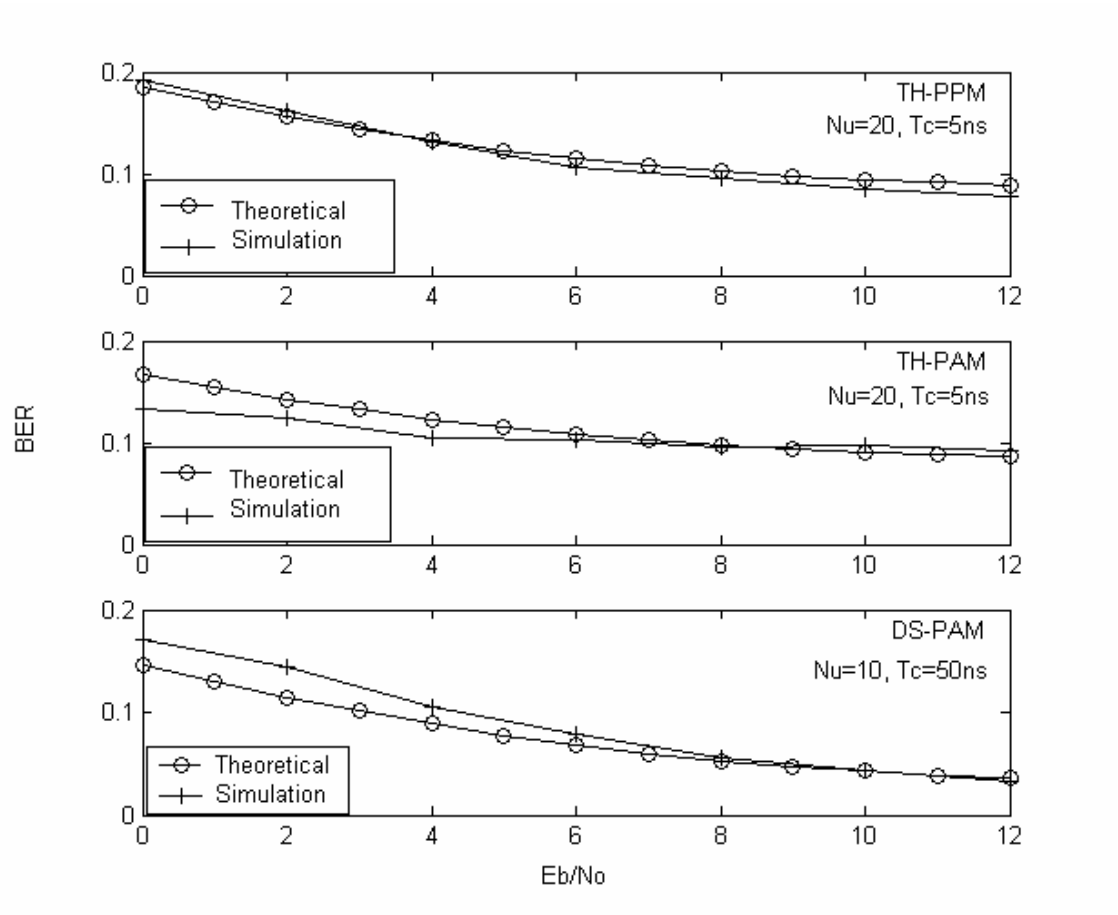

Fig. 4.1 Fading channel performance comparison of theoretical and simulation results

PERFORMANCE OF M-ARY TH-PAM/PPM SCHEMES IN AWGN CHANNELS

In chapters 3 and 4 we have dealt with binary UWB systems. In this chapter, exact statistical modeling of multiple access interference (MAI) for M-ary TH-PAM and TH-PPM ultra wideband systems are presented. Based on these models the exact symbol error rate (SER) is expressed in simple formulas for TH-PAM. For TH-PPM an approximate expression and an upper bound for the SER are presented.

5.1 M-ary System model

An M-ary symbol is encoded in to the TH pulse sequence either by adjusting the pulse positions or by changing the amplitudes. The j^{th} transmitted symbol of user u is denoted by D_j^u .

5.1.1 M-ary TH-PAM

In an M-ary TH-PAM system the data symbols are defined as follows

$$D_j^u \in \{2m-1-M\}_{m=1}^{M}. \tag{5.1}$$

The transmitted signal of the u^{th} user, $v_u(t)_{M-PAM}$ is defined by

$$v_u(t)_{M-PAM} = \sqrt{E}\sum_{i=0}^{\infty} D_{\lfloor i/Ns \rfloor}^u w\left[t - iT_f - C_i^u T_c\right]. \tag{5.2}$$

The correlating template waveform $b_T(t)_{M-PAM}$ used for the detection of the j^{th} symbol of the 0^{th} user is defined as follows

$$b_T(t)_{M-PAM} = \sum_{i=jN_s}^{(j+1)N_s-1} w\left(t - iT_f - C_i^0 T_c\right). \tag{5.3}$$

The decision variable r obtained at the correlator output is given by

$$r = \int_{jT_s}^{(j+1)T_s} b_T(t-\tau^0)_{M-PAM}\, r(t)\; dt = s_{M-PAM} + I_{M-PAM} + n_{M-PAM}\,, \qquad (5.4)$$

where the signal component s_{M-PAM} is given by

$$s_{M-PAM} \in \{(2m-1-M)\,N_s\sqrt{E}R_{ww}(0)\}_{m=1}^{M} \qquad (5.5)$$

And the MAI component can be given by

$$I = \int_{jT_s}^{(j+1)T_s} b_T(t-\tau^0)_{M-PAM} \sum_{u=1}^{N_u-1} v_u(t-\tau^u)_{M-PAM}\, dt\,. \qquad (5.6)$$

Here, $T_s = N_s T_f$ is the symbol duration. Finally, the decision rule for M-ary TH-PAM is given by

$$D_j^u = \underset{m\in\{2m-M-1\}_{m=1}^{M}}{\arg\min} \left(|r - s_m|\right), \qquad (5.7)$$

where s_m represents the m^{th} signal component in (5.5).

5.1.2 M-Ary TH-PPM

In an M-ary TH-PPM system the data symbols can be defined as follows

$$D_j^u \in \Big\{0,1,.....,M-1\Big\}. \qquad (5.8)$$

The m^{th} symbol is represented by shifting its origin by $m\delta$ in the time axis, where δ is taken as the basic modulation step. Therefore the transmitted signal $v_u(t)_{M-PPM}$ is given by

$$v_u(t)_{M-PPM} = \sqrt{E}\sum_{i=0}^{\infty} w\left[t - iT_f - C_i^u T_c - \delta D^u_{\lfloor i/Ns \rfloor}\right]. \qquad (5.9)$$

M-ary TH-PPM uses a bank of M correlators for detection, where the template waveform of the m^{th} correlator of user 0 is defined by

$$b_T^m(t)_{M-PPM} = \sum_{i=jN_s}^{(j+1)N_s-1} w\big(t - iT_f - C_i^0 T_c - m\delta\big). \qquad (5.10)$$

The decision variable at the output of the m^{th} correlator detector of the M-ary PPM receiver is given by

$$r_m = \int_{jT_s}^{(j+1)T_s} b_T(t-\tau^0)_{M-PPM}\, r(t)\, dt = s^m_{M-PPM} + I^m_{M-PPM} + n^m_{M-PPM}, \qquad (5.11)$$

where the desired signal component s^m_{M-PPM} is given by

$$s^m_{M-PPM} \in \left\{0,\ N_s\sqrt{E}R_{ww}(0)\right\}. \qquad (5.12)$$

s^m_{M-PPM} will assume the value $N_s\sqrt{E}R_{ww}(0)$ only when if transmitted symbol's index is m. The MAI component from the m^{th} correlator is given by

$$I^m_{M-PPM} = \int_{jT_s}^{(j+1)T_s} b^m_T(t-\tau^0)_{M-PPM} \sum_{u=0}^{N_u-1} v_u(t-\tau^u)_{M-PPM}\, dt. \qquad (5.13)$$

Finally the decision rule is given by

$$D^u_j = \underset{m\in\{0,1,2.....,M\}}{\arg\max}\ (r_m). \qquad (5.14)$$

5.2 Multiple access interference model

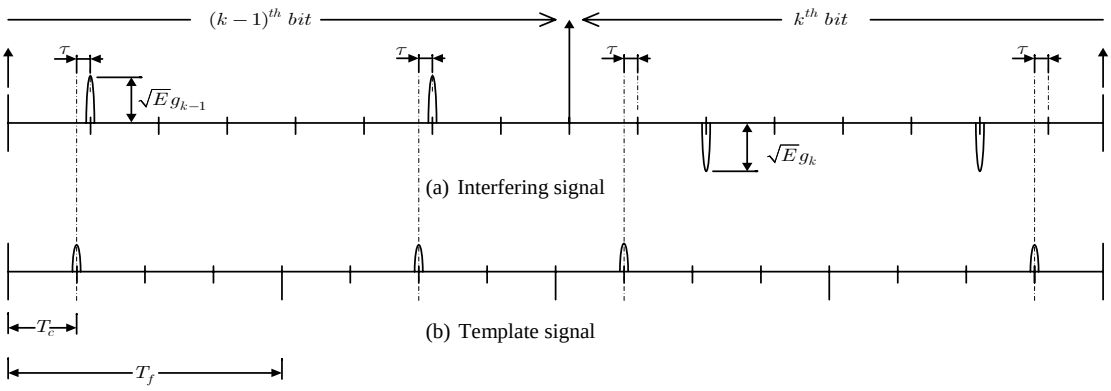

Fig. 5.1 An interfering signal (a) compared against the template waveform (b) of the desired user with $N_f = 4$ and $T_c = T_f / 4$ for M-ary TH-PAM

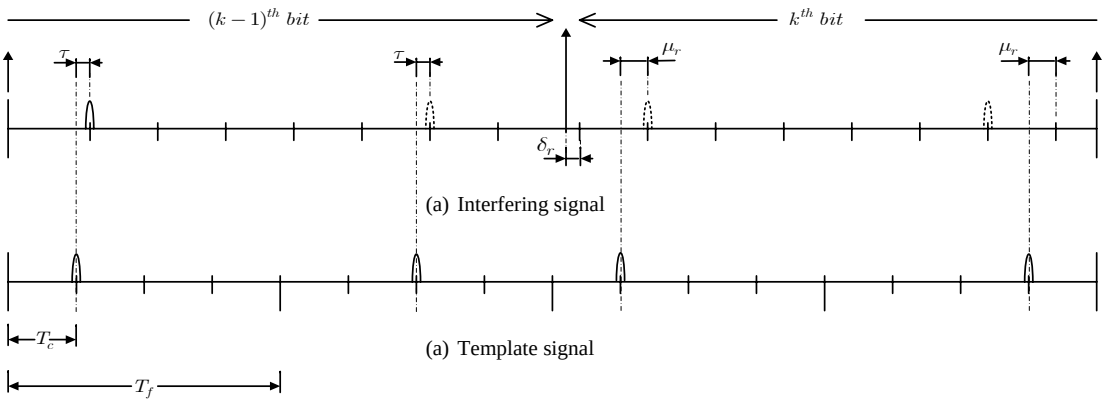

Fig. 5.2 An interfering signal (a) compared against the template waveform (b) of the desired user with $N_f = 4$ and $T_c = T_f / 4$ for M-ary TH-PPM

In Fig. 5.1 and Fig. 5.2 the template signals are compared against typical interfering signals. τ has the similar definition as in chapter 3. Therefore, for a given value of τ the total interference over the symbol duration of user u can be written as

$$I^{u}{}_{/\tau} = n_1\Omega_0 + n_2\Omega_1, \tag{5.15}$$

where n_1 and n_2 are integers with, $n_1 \le N_s$, $n_2 \le N_s$ and $n_1 + n_2 \le N_s$, respectively representing the number of pulses overlapping in $(k-1)^{th}$ and k^{th} symbol durations. The components Ω_o, Ω_1 are defined for M-ary TH-PAM and M-ary TH-PPM as follows:

For M-ary TH-PAM:

$$\Omega_0 = g_{k-1}R_{ww}(\tau) \text{ and } \Omega_1 = g_k R_{ww}(\tau), \tag{5.16}$$

where $g_{k-1}, g_k \in \{2m-1-M\}_{m=1}^{M}$ are equiprobable independent random variables representing the $(k-1)^{th}$ and k^{th} symbols, respectively. The pair, g_{k-1}, g has M^2 possible values, each of these values has a probability of occurrence $1/M^2$.

For M-ary TH-PPM:

$$\Omega_0 = R_{ww}(\tau) \text{ and } \Omega_1 = R_{ww}(\mu_r), \tag{5.17}$$

where μ_r represents the distance from a template pulse to its closest pulse origin in the interfering signal (defined in the k^{th} symbol region (Fig 5.2)). It can be shown that μ_r is equal to the value which has the lowest magnitude among $\left[(\tau+\delta_r),(\tau+\delta_r-T_c),(\tau+\delta_r+T_c)\right]$, where δ_r is defined as the relative shift between the two sets of pulse origins (recall that the pulse origins are divided into two sets, corresponding to $(k-1)^{th}$ and k^{th} symbol durations). From the definition of δ_r it is obvious that, $\delta_r \in \{-(M-1)\delta...,0,...,(M-1)\delta\}$. Therefore, it can be shown that δ_r has the following probability of occurrence

$$P_{\delta_r}(\delta_r = j\delta) = \left(\frac{M-|j|}{M^2}\right). \tag{5.18}$$

In both M-ary modulation schemes, the statistical modeling of I^u is completed by evaluating the corresponding probabilities of the discrete values of $I^u{}_{/\tau}$ and using the distribution of τ. Similar to the binary modulation case, the following probability function $P(n_1,n_2)$ is defined, with respect to the possible values of $I^u{}_{/\tau}$ in (5.15).

$$P(n_1,n_2) = P(I^u{}_{/\tau} = n_1\Omega_0 + n_2\Omega_1), \tag{5.19}$$

The equation for $P(n_1,n_2)$ can be derived as shown below:

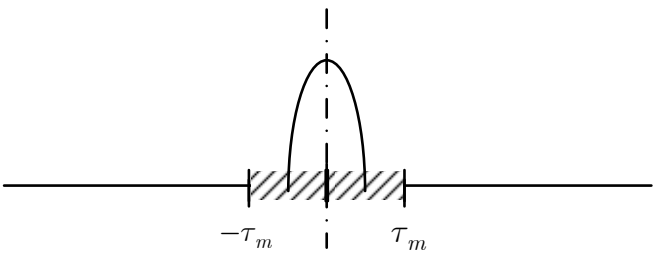

Fig. 5.3 A sample mono-pulse waveform of the M-ary template pulse

Fig. 5.3 is an enlarged version of a single mono-pulse in the desired user's template signal. (here, we have selected the first template pulse without loss of generality). Due to the bit changeover, the template pulses in the desired user signal are divided in to two sets, each having $m_{(k-1)}$ and $m_{(k)}$ number of template pulses respectively, where $m_{(k-1)} + m_{(k)} = N_s$. Since the position of bit changeover is a uniform random variable, each value that the pair $m_{(k-1)}, m_{(k)}$ can take, has an average probability equal to $1/N_s$. The interference contribution from the $(k-1)^{th}$ bit and the $(k)^{th}$ bit are, $n_1\Omega_1$ and $n_2\Omega_2$ respectively. By considering the available combinations for all the possible bit changeover positions (5.19) can be written as

$$P(n_1, n_2) = \sum_{j=(n_1-1)}^{(N_s-n_2-1)} \frac{1}{N_s} C_{n_1}^{(j+1)} (1/N_h)^{n_1} (1 - 1/N_h)^{(j-n_1+1)} \cdot C_{n_2}^{(N_s-j-1)} (1/N_h)^{n_2} (1 - 1/N_h)^{(N_s-j-n_2-1)}. \quad (5.20)$$

5.3 Derivation of the CF and SER

5.3.1 M-ary TH-PAM

For TH-PAM $\Phi_{(I^u)}(w)$ can be expressed as,

$$\Phi_{(I^u)}(w) = \frac{1}{T_c} \int_{-\tau_m}^{\tau_m} \Phi_{(I^u/\tau)} d\tau + P_0, \quad (5.21)$$

$$\Phi_{(I^u/\tau)} = \sum_{n_1=0}^{Ns} \sum_{n_2=0}^{Ns-n_1} \sum_{g_{k-1}} \sum_{g_k} \frac{1}{M^2} P(n_1, n_2) \exp\left(jw \left(n_1 g_{k-1} + n_2 g_k \right) R_{ww}(\tau) \right), \quad (5.22)$$

Note that the notation $\sum_{g_k}$ represents the summation over the possible values of g_k.

By separating the zero interference probability P_0 in (5.21), the range of integration is reduced to $[-\tau_m, \tau_m]$, where P_o is given by $(1 - 2\tau_m / T_c)$. Equation (5.22) is the

CF of I^u, conditioned on τ. Since we assume that positive and negative symbols are equally probable, the distribution of I^u becomes symmetric. Hence, we can write,

$$\Phi_{(I^u)}(w) = \Phi_{(-I^u)}(w) = \frac{1}{2}\big(\Phi_{(I^u)}(w) + \Phi_{(-I^u)}(w)\big). \tag{5.23}$$

By applying (5.23), to get rid of the complex integration in (5.21), we get the following real valued expressions, which will be more convenient in performing numerical integrations.

$$\Phi_{(I^u)}(w) = \frac{1}{2T_c}\int_{-\tau_m}^{\tau_m} \Phi' \, d\tau + P_0 \,, \tag{5.24}$$

$$\Phi' = \sum_{n_1=0}^{Ns} \sum_{n_2=0}^{Ns-n_1} \sum_{g_{k-1}} \sum_{g_k} \frac{1}{M^2} P(n_1, n_2) \cos\big(w\big(n_1 g_{k-1} + n_2 g_k\big) R_{ww}(\tau)\big). \tag{5.25}$$

Since I^u are independent to each other, $\Phi_I(w)$ is given by

$$\Phi_I(w) = [\Phi_{I^u}(w)]^{N_u - 1} \qquad . \tag{5.26}$$

The CF of the AWGN component (n_{M-PAM}) is given by, $\Phi_{n_{M-PAM}}(w) = \exp\left(\frac{-w^2 N_o R_{ww}(0) N_s}{4}\right)$.

Now the average SER of the M-ary modulation scheme can be given by,

$$P_e = \frac{2(M-1)}{M} P\big(I + n \geq \sqrt{E} N_s R_{ww}(0)\big) \tag{5.27}$$

Therefore P_e can be expressed in the following form,

$$P_e = \frac{2(M-1)}{M}\left(\frac{1}{2} - \frac{1}{2\pi}\int_{-\infty}^{\infty} \frac{\Phi_I(w)}{jw} \Phi_n(w) e^{j\left(w\sqrt{E} N_s R_{ww}(0)\right)} dw\right). \tag{5.28}$$

By the symmetry of the distribution of I and by using the substitution $w_o = \sqrt{E} w$, the integral reduces to a convenient real function form as,

$$P_e = \frac{2(M-1)}{M}\left[\frac{1}{2} - \frac{N_s R_{ww}(0)}{\pi}\int_0^{\infty} \Phi_{I_N}(w_o)\exp\left(\frac{w_o^2 N_s^2 R_{ww}^2(0)\left(M^2-1\right)}{12\gamma \log_2 M}\right)\right. \tag{5.29}$$
$$\left.\operatorname{sinc}\left(\frac{N_s R_{ww}(0) w_o}{\pi}\right) dw_o\right]$$

where $\Phi_{I_N}(w_o)$ is the CF of the normalized interference and is given by,

$$\Phi_{I_N}(w_o) = E\left\{e^{jw_o\left(\frac{I}{\sqrt{E}}\right)}\right\}, \tag{5.30}$$

and $\gamma = \frac{E_b^{av}}{N_o}$. E_b^{av} represents the average bit energy and is given by $E_b^{av} = \frac{M^2-1}{3\log_2 M} E N_s R_{ww}(0)$.

5.3.2 M-ary TH-PPM

In an M-ary TH-PPM system, $\Phi_{(I^u)}(w)$ can be expressed as

$$\Phi_{(I^u)}(w) = \frac{1}{T_c}\int_{-T_c/2}^{T_c/2} \Phi_{(I^u/\tau)} d\tau \ , \tag{5.31}$$

where

$$\Phi_{(I^u/\tau)} = \sum_{n_1=0}^{Ns}\sum_{n_2=0}^{Ns-n_1}\sum_{\delta_r} P_{\delta_r}(\delta_r) P(n_1,n_2)\exp\left(jw\left(n_1 R_{ww}(\tau) + n_2 R_{ww}(\mu_r)\right)\right) \tag{5.32}$$

Since all the M symbols are equiprobable, the average SER is equal to the SER of an individual symbol. We assume that the first symbol is transmitted. Therefore, $r_1 = N_s\sqrt{E}R_{ww}(0) + I^1_{M-PPM} + n^1_{M-PPM}$, and $r_m = I^m_{M-PPM} + n^m_{M-PPM}$ for $m \geq 2$. It should be noted that $I^m_{M-PPM} + n^m_{M-PPM}$ follows the same distribution irrespective of m.

The SER of the first symbol can be given by $P_e = \int_{-\infty}^{\infty} P^1_{e/r_1} P(r_1)\, dr_1$, where P_e^1 is the

probability of error when the first symbol is transmitted. The conditional probability P^1_{e/r_1} can be given by $P^1_{e/r_1} = 1 - P((r_1 > r_2),(r_1 > r_3),.....,(r_1 > r_M) \mid r_1)$. By taking the assumption that r_m's are i.i.d random variables for $m \geq 2$, SER can be estimated as follows

$$P_e = \int_{-\infty}^{\infty} \left(1 - (F(r_1))^{M-1}\right) P(r_1) dr_1, \tag{5.33}$$

where $F(.)$ is the CDF of r_m for $m \geq 2$.

But, notably the numerical evaluation of this equation is complex; therefore the following loose upper bound is presented as an alternative:

$$P^1_{e/r_1} \leq \sum_{i=2}^{M} P(r_1 < r_i \mid r_1) = (M-1) P(r_1 < r_2 \mid r_1) . \tag{5.34}$$

This implies

$$P_e \leq \int_{-\infty}^{\infty} (M-1)(1 - F(r_1)) P(r_1) dr_1 . \tag{5.35}$$

The CDF of r_2 ($F(.)$) can be related to its CF by

$$F(r_1) = \frac{1}{2} + \frac{1}{2\pi} \int_{-\infty}^{\infty} \frac{\Phi_{r_2}(-w)}{jw} e^{jwr_1} dw \tag{5.36}$$

But $\Phi_{r_2}(w) = \Phi_I(w)\Phi_n(w)$, where $\Phi_I(w)$ is the CF of I^m_{M-PPM} and $\Phi_n(w)$ is the CF of n^m_{M-PPM}. Therefore we get

$$F(r_1) = \frac{1}{2} + \frac{1}{2\pi} \int_{-\infty}^{\infty} \frac{\Phi_I(-w)\Phi_n(-w)}{jw} e^{jwr_1} dw \tag{5.37}$$

Substituting this in to the right side of (5.35) gives

$$P_e \le \frac{M-1}{2}\left(1-\frac{1}{\pi}\int_{-\infty}^{\infty}\frac{\Phi_I(-w)\Phi_n(-w)}{jw}\Phi_{r_1}(w)dw\right)$$
$$\le \frac{M-1}{2}\left(1-\frac{1}{\pi}\int_{-\infty}^{\infty}\frac{|\Phi_I(w)|^2\Phi_n^2(w)}{jw}e^{jws}dw\right) \quad , \qquad (5.38)$$

where $s = N_s\sqrt{E}R_{ww}(0)$. Note that $\Phi_{r_1}(w) = \Phi_I(w)\Phi_n(w)e^{jws}$.

5.4 Numerical results

The pulse waveform given in (3.45) is used to obtain these results. And the parameter values used are $\tau_m = 0.5ns$, $N_h = 12$ and $N_u = 25$. Fig 5.4 shows the comparison of theoretical and simulation results for M-ary TH-PAM for different values of M. The theoretical results agree well with the simulation curves.

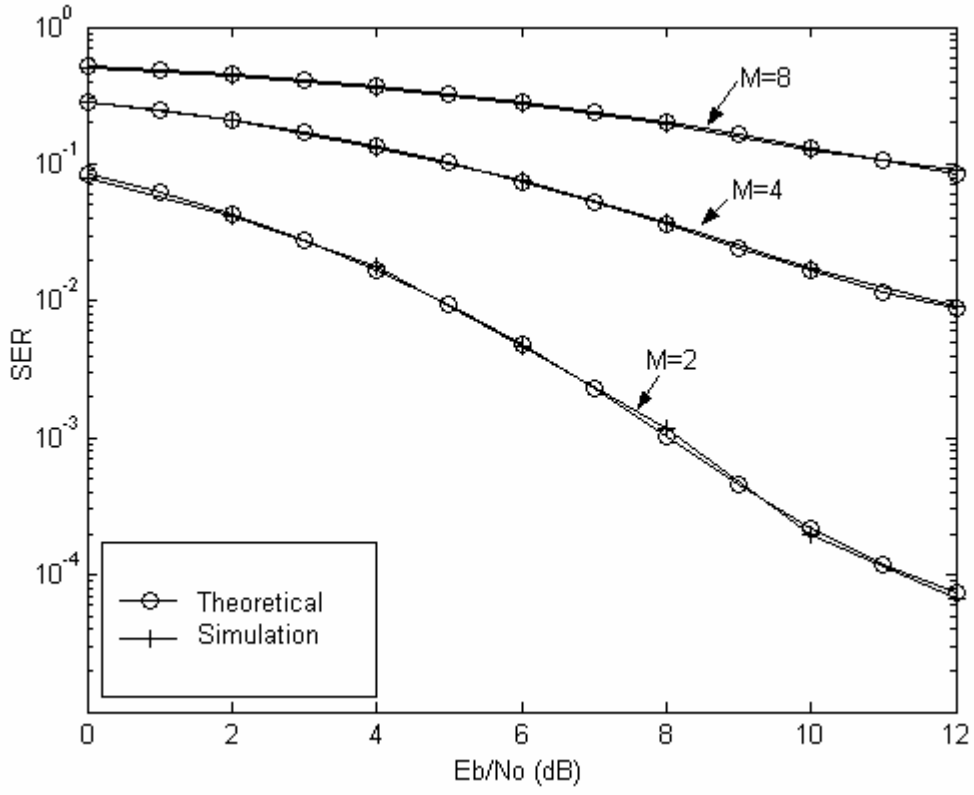

Fig. 5.4 Performance of M-ary TH-PAM depicted for $N_s = 8$, with $T_c / \log_2(M) = 2ns$ and $\delta = 0.135ns$.

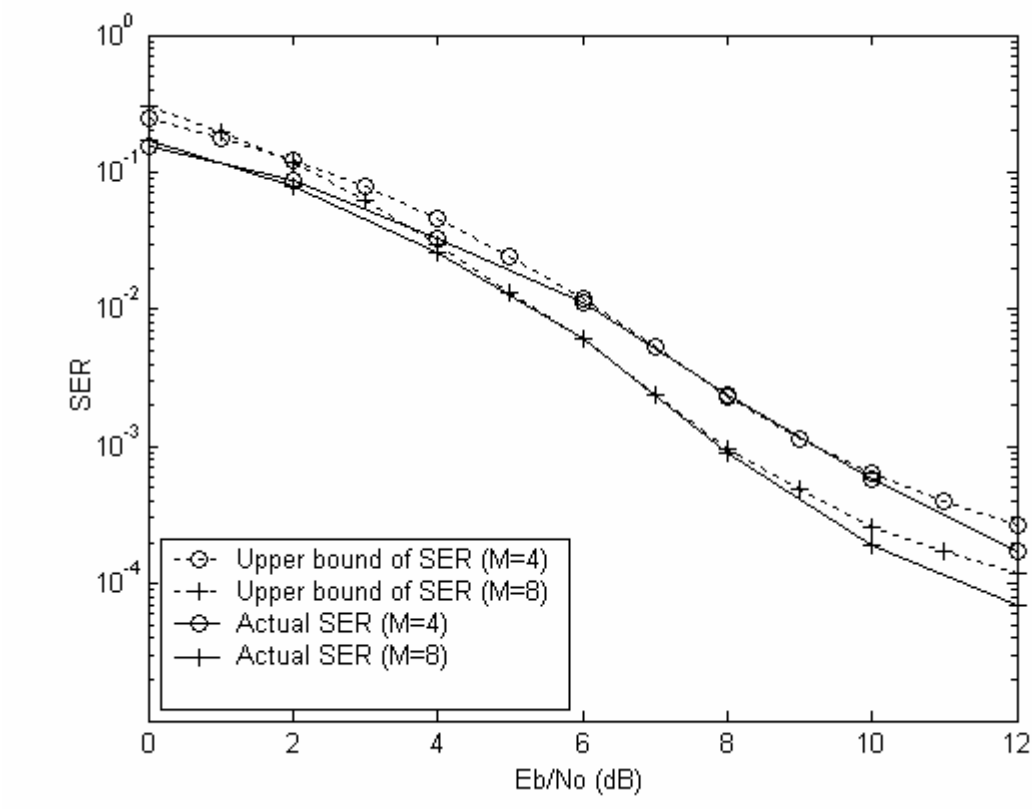

Fig. 5.5 Performance of M-ary TH-PPM using the upper bound probability, depicted for $N_s = 8$, with $T_c / \log_2(M) = 2ns$ and $\delta = 0.135ns$.

In Fig. 5.5, the upper bound probability is plotted against the simulation results for M-ary TH-PPM. The bound is closer to the actual SER values at higher E_b / N_o ratios. For PAM the performance is high at $M = 2$ and it reduces with increasing M. In the case of PPM, since the M signals are orthogonal the performance improves with M.

5.5 Conclusion

The exact statistical modeling of MAI in AWGN channel is presented for M-ary TH-PAM and TH-PPM UWB systems. This model is implemented by evaluating the corresponding probabilities. The CF of the MAI for M-ary PAM is also derived. For M-ary PPM, CF of MAI for each branch can be derived exactly. With the help of this, exact SER of M-ary PAM is expressed in simple closed forms. For M-ary PPM an upper bound for the SER is provided.

PERFORMANCE IMPROVEMENT BY AN ADAPTIVE TRANSMIT ARRAY

In this chapter, a novel technique to improve the performance of an UWB-IR system is presented. This technique is based on the idea of coherent combining of electromagnetic signals in space by using an array of M adaptive transmitters. Proposed system's performance is evaluated by simulations in indoor multi-path channel and is compared with receiver diversity. Possibility of using RAKE reception with the proposed scheme is also discussed in this chapter. The system model and numerical results are provided for binary TH-PPM as an example, but the scheme is suitable for TH-PAM and DS-PAM as well.

6.1 Introduction

Performance of UWB-IR is significantly downgraded by multiple access interference (MAI), multipath interference (MPI), shadowing and fading in the indoor channel. MAI increases proportionately with the number of active users and the rest are dependant on the channel's scattering pattern.

Multipath diversity is already available in the UWB channel due to the rich scattering and large number of resolvable multipaths. Exploiting this multipath diversity, selective maximal ratio combiners (or S-RAKE receivers) [46] increase the performance by combining the energy from selected strong paths. Performance of RAKE reception in spread spectrum systems operating in dense multipath

environments is studied in [47- 48]. Also it was shown, using a constant power delay profile, that the increase in performance by adding another path's energy is significantly small as the number of RAKE fingers grow. This effect will be even more significant in indoor wireless channels, since the power delay profile is an exponentially decaying function [9], [12]. On the other hand, the complexity of the receiver grows proportionally whilst providing only a small gain in performance. Therefore, it is important to find other techniques to improve the UWB-IR system performance with acceptable level of receiver complexity.

Antenna diversity is a widely known technique to mitigate the effect of multipath fading and hence to improve the performance [49]. Receiver diversity becomes an inappropriate candidate for wireless hand-held devices and small scale indoor wireless applications as it increases the cost, hardware complexity and the form factor of the receiver. Also the separations between the antennas should be kept large enough to eliminate signal correlation which is not practically attractive for UWB-IR. But on the other hand, transmit (TX) diversity can be more attractive if a centralized network architecture is used.

A simple space-time coding scheme was proposed in [50] for UWB-IR in flat fading (FF) channel. The assumption of a FF channel is the main drawback in [50], and simple linear combining techniques are not feasible in highly time dispersive UWB indoor channels due to the different arrival times of signals from the antennas in the array.

6.2 Coherent combining

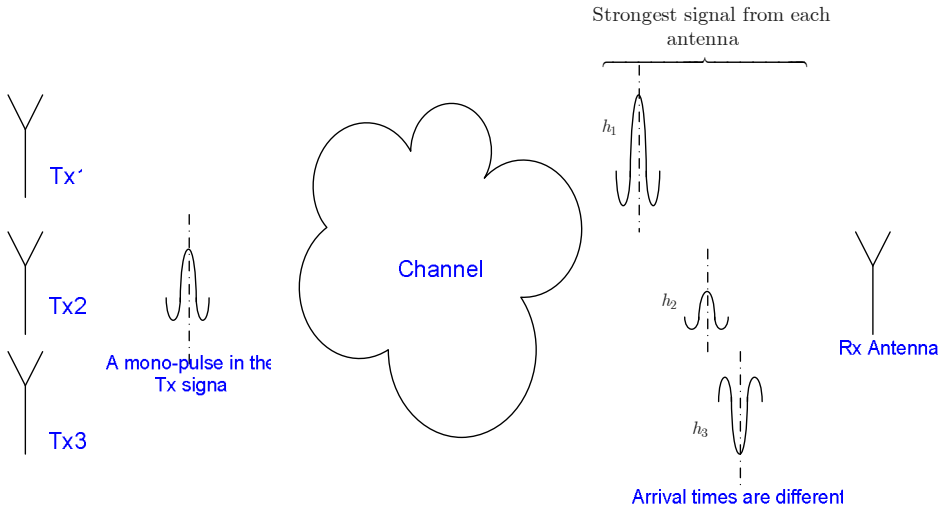

Figure 6.1 Signals before coherent combining

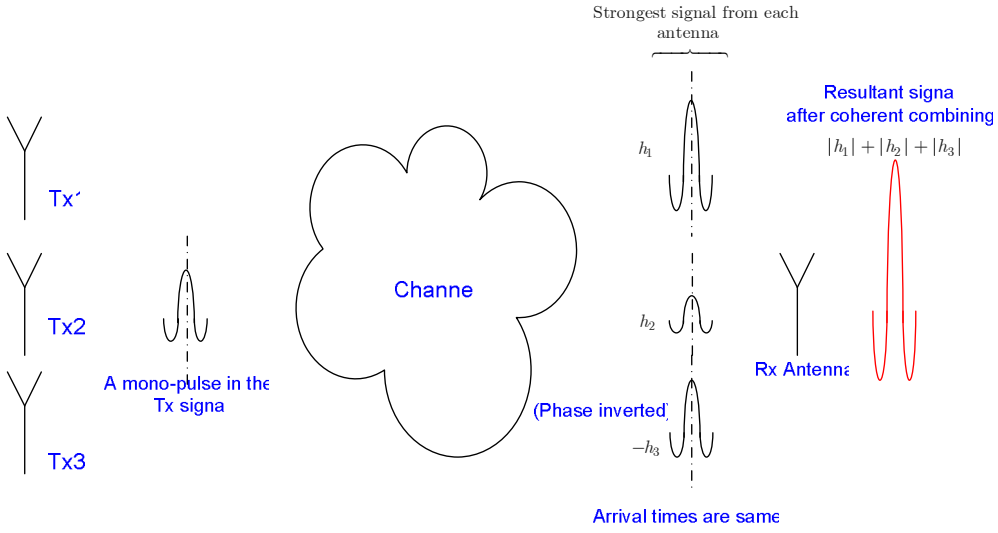

Figure 6.2 Signals after coherent combining

Combining electromagnetic signals in space coherently and constructively is named as coherent combining. The total signal strength in a region in space (spot) can be increased by summing a number of replicas of the signal, which are transmitted from an array of antennas. Coherent arrival of these replicas at the 'spot' can be achieved by

proper delay adjustments at the transmit array. If the received signal undergoes polarity reversal due to the effect of the channel, polarity adjustments are needed at the array to achieve constructive combining. The idea is illustrated in Fig. 6.2 and Fig. 6.3.

Funk and Lee [51] presented an experimental demonstration of the coherent addition of UWB pulsed radiation in free space. It is also shown that the received peak power scales as M^2 in free space, if an array of M antennas is used. This is due to the superposition of M equal strength electromagnetic pulses. Using the same concept, a space time array to illuminate a localized region in space was presented in [52] for cancer treatment applications.

6.3 Coherent combining TH-PPM array

Coherent combining can be used to improve the performance of UWB-IR. In order to achieve constructive combining, polarity adjustments are needed with delay adjustments since the UWB signal undergoes polarity reversals due to reflections [9].

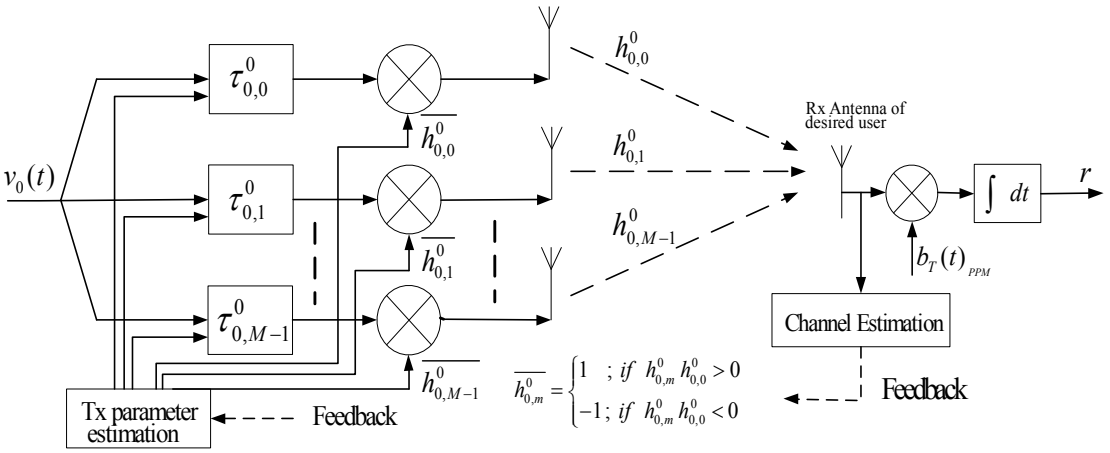

Fig. 6.3. Block diagram of the coherent combining transmit array

Fig. 6.3. shows the block diagram of the proposed TX diversity scheme. It should be noted that the transmitted power is scaled down by M, the number of TX antennas in the array, to maintain the total transmitted power constant. Let us define $v_u'(t)_{PPM} = \frac{1}{\sqrt{M}} v_u(t)_{PPM}$, where $v_u(t)_{PPM}$ is defined by (2.2). Therefore the received signal before delay-tuning is given by

$$r(t) = \sum_{m=0}^{M-1} \sum_{u=0}^{Nu-1} \sum_{l=0}^{L-1} h_{l,m}^{u} \times v_u' \left(t - \tau_{l,m}^{u} \right)_{PPM} + n(t) \tag{6.1}$$

The additional subscript m in $h_{l,m}^{u}$ and $\tau_{l,m}^{u}$ represents the respective TX antenna. It is assumed that the paths are indexed in descending order of their strengths.

The delay of the strongest path to the desired (i.e $u = 0$) user, from each antenna, is estimated at the receiver. Then, each antenna's transmitted signal is forwarded by this delay in order to tune the array to the desired user. And the transmitting polarity is also corrected so that the received signals through all the M strongest paths have the same polarity. In the practical scenario, the signals should be delayed further to match with the longest delay. However we assume that the signals are forwarded in time for the simplicity of our equations. Forwarding in time is hypothetical but the model is still the same, except a change in the time reference. Now, the received signal after the adjustments becomes,

$$r(t) = [s(t) + c(t) + m(t) + n(t)] \tag{6.2}$$

where $s(t)$ is the useful signal component and is given by

$$s(t) = \left[\sum_{m=0}^{M-1} \widehat{h_{0,m}^{0}} \times v_0'(t)_{PPM} \right], \tag{6.3}$$

$c(t)$ is the self (multipath) interference and is given by

$$c(t) = \left[\sum_{m=0}^{M-1} \sum_{l=1}^{L-1} \widehat{h_{l,m}^{0}} \times v_0^{'} \left(t - \tau_{l,m}^{0} + \tau_{0,m}^{0} \right)_{PPM} \right], \tag{6.4}$$

and $m(t)$ is the multiuser interference and is given by

$$m(t) = \left[\sum_{u=1}^{Nu-1} \sum_{m=0}^{M-1} \sum_{l=0}^{L-1} \widehat{h_{l,m}^{u}} \times v_u^{'} \left(t - \widehat{\tau_{l,m}^{u}} \right)_{PPM} \right]. \tag{6.5}$$

The gain coefficients after adjustment are given by

$$\widehat{h_{0,m}^{0}} = \mid h_{0,m}^{0} \mid \frac{h_{0,0}^{0}}{\mid h_{0,0}^{0} \mid}, \text{ and} \tag{6.6}$$

$$\widehat{h_{l,m}^{0}} = h_{l,m}^{0} \frac{\widehat{h_{0,m}^{0}}}{h_{0,m}^{0}}, \quad \forall l \neq 1 . \tag{6.7}$$

Note that $\widehat{h_{0,m}^{0}}$ and $h_{0,m}^{0}$ differ only by the sign. For $u > 0$, $\widehat{h_{l,m}^{u}}$ and $\widehat{\tau_{l,m}^{u}}$ depends on the adjustments related to the u^{th} receiver. It should be noted that the required channel parameters, the polarity of $h_{0,m}^{u}$ and the differential delay $\tau_{0,m}^{u}$, are estimated at the receiver and fed back to the TX array through a feedback path.

6.4 Performance in AWGN channel

In an AWGN channel, the received signal in (6.2) becomes,

$$r(t) = M v_0(t)_{PPM} + \sum_{m=0}^{M-1} \sum_{u=1}^{Nu-1} v_u^{'}(t - \widehat{\tau_m^{u}})_{PPM} + n(t). \tag{6.8}$$

Suffix l is eliminated since there is no multipath involved. The receiver is a single correlator (or matched filter) detector, where the correlating template waveform, $b_T(t)_{PPM}$ for the detection of the j^{th} bit is given in (2.5). Thus the correlator output r is given by

$$r = \int_{jT_b}^{(j+1)T_b} b_T(t)_{PPM} \times r(t) dt . \tag{6.9}$$

The decision rule becomes, $"Decide" \begin{cases} D_j = 0 \Leftrightarrow r > 0 \\ D_j = 1 \Leftrightarrow r < 0 \end{cases}$,

Simplifying r yields, $r = s + I + n$; where $s = M\sqrt{\frac{EN_s^2}{M}} = \sqrt{MEN_s^2}$,

$$I = \int_{jT_b}^{(j+1)T_b} b_T(t)_{PPM} \sum_{m=0}^{M-1} \sum_{u=1}^{Nu-1} v_u'(t - \widehat{\tau_m^u})_{PPM} \, dt \tag{6.10}$$

and

$$n = \int_{jT_b}^{(j+1)T_b} n(t) b_T(t)_{PPM} dt \ . \tag{6.11}$$

Since I, n are independent the signal to interference ratio (SIR) becomes

$$SIR = \frac{MEN_s^2}{\sigma^2 + \sigma_I^2}, \tag{6.12}$$

where $\sigma^2 = E(n^2)$ and $\sigma_I^2 = E(I^2)$. In a singleuser environment (6.12) becomes $SIR = MEN_s^2 / \sigma^2$, which shows an M fold increase compared to the SIR in a single antenna scheme which is EN_s^2 / σ^2. But in a multi RX scheme with M receive antennas SIR is given by, $\frac{(M\sqrt{E}N_s)^2}{M\sigma^2} = MEN_s^2 / \sigma^2$. This predicts that the performance of the proposed scheme and a multi RX scheme are similar in singleuser AWGN environment.

6.5 Multiuser performance in multipath fading channel

6.5.1 Detection using a single correlator receiver

In a multipath channel the correlator output, r becomes

$$r = \int_{jT_b}^{(j+1)T_b} r(t) \times b_T^{'}(t)_{PPM}\, dt = s + \underbrace{MAI + MPI}_{I} + n\,, \tag{6.13}$$

where $b_T^{'}(t)_{PPM} = \dfrac{h_{0,0}^0}{|\, h_{0,0}^0\,|} b_T(t)_{PPM}$,

$$s = \int_{jT_b}^{(j+1)T_b} \left[\sum_{m=0}^{M-1} \widehat{h_{0,m}^0} \times v_0^{'}(t)_{PPM} \right] b_T^{'}(t)_{PPM}\, dt\,, \tag{6.14}$$

$$MPI = \int_{jT_b}^{(j+1)T_b} \left[\sum_{m=0}^{M-1} \sum_{l=1}^{L-1} \widehat{h_{l,m}^0} \times v_0^{'}\left(t - \tau_{l,m}^0 + \tau_{0,m}^0\right)_{PPM} \right] b_T^{'}(t)_{PPM}\, dt\,, \tag{6.15}$$

$$MAI = \int_{jT_b}^{(j+1)T_b} \left[\sum_{m=0}^{M-1} \sum_{u=1}^{N_u-1} \sum_{l=0}^{L-1} \widehat{h_{l,m}^u} \times v_u^{'}\left(t - \widehat{\tau_{l,m}^u}\right)_{PPM} \right] b_T^{'}(t)_{PPM}\, dt\,. \tag{6.16}$$

s can be further simplified as

$$\begin{aligned} s &= \left[\sum_{m=0}^{M-1} \widehat{h_{0,m}^0} \right] \int_0^{T_b} v_0^{'}(t) \times b_T^{'}(t)_{PPM}\, dt \quad] \\ &= (-1)^{D_j} \sqrt{\frac{EN_s^2}{M}} \left[\sum_{m=0}^{M-1} |\, h_{0,m}^0\,| \right] \end{aligned}\,, \tag{6.17}$$

where the sign of s is determined by D_j.

Let's define $\sigma_I^2 = E\{(MAI + MPI)^2\}$, where $E(MAI + MPI) = 0$ as negative and positive path gains are equiprobable due to reflections [9]. The level of interference (I) is unchanged with the number of transmit antennas. This can be understood by seeing each antenna's contribution to the total interference as M identically and independently distributed random variables, where each variable's second moment($E\{(.)^2\}$) is scaled down by M (as we scale down the TX power by M). See section 6.7 for more details.

Therefore, SIR of the proposed scheme, SIR_P becomes

$$SIR_P = \frac{s^2}{\sigma^2 + {\sigma_I}^2}$$

$$= \frac{\frac{EN_s^2}{M}\left[(-1)^{D_j}\left[\sum_{m=0}^{M-1} \mid h_{0,m}^0 \mid\right]\right]^2}{\sigma^2 + {\sigma_I}^2}. \qquad (6.18)$$

$$= \frac{\frac{EN_s^2}{M}\left[\sum_{m=0}^{M-1} \mid h_{0,m}^0 \mid\right]^2}{\sigma^2 + {\sigma_I}^2}$$

6.5.2 Detection by RAKE reception after coherent combining

In section 6.5.1 only the energy in the coherently combined path was considered for detection without exploiting the diversity available from other paths. In this section, we consider RAKE reception with coherent combining (post-combining RAKE reception). After selecting the combined path which is generally the strongest path with the signal gain $h_0 = \frac{h_{0,0}^0}{\mid h_{0,0}^0 \mid}\sum_{m=0}^{M-1} \mid h_{0,m}^0 \mid$ and the delay $\tau_0 = 0$, we select another $P-1$ number of significant paths from the remaining $M \times (L-1)$ paths. Let h_p and τ_p are their corresponding path gains and delays respectively for $i = 1, 2, 3...., P-1$. In this case the decision metric ζ with maximal ratio combining (MRC) becomes

$$\zeta = \sum_{p=0}^{P-1}\left[h_p \int_{jT_b}^{(j+1)T_b} r(t) \times b_T(t-\tau_p)_{PPM}\, dt\right]. \qquad (6.19)$$

The signal component in (6.19) is given by $s = \sqrt{\frac{EN_s^2}{M}} \sum_{p=0}^{P-1} (h_p)^2$. Therefore, the SIR for this case becomes

$$SIR_{P-Rake} = \frac{s^2}{(\sigma^2 + {\sigma_I}^2) \sum_{p=0}^{P-1} (h_p)^2}$$

$$= \frac{\frac{EN_s^2}{M} \sum_{p=0}^{P-1} (h_p)^2}{\sigma^2 + {\sigma_I}^2} \quad . \tag{6.20}$$

$$= \frac{\frac{EN_s^2}{M} \left[\left[\sum_{m=0}^{M-1} | h_{0,m}^0 | \right]^2 + {h_1}^2 + ..{h_{P-1}}^2 \right]}{\sigma^2 + \sigma_I^2}$$

It can be noticed that (6.20) shows an increase compared to (6.18). However, the increase in performance due to this increment will be determined by the magnitude of h_0. As h_0 grows large with increasing M, the increase in SIR_{P-Rake} becomes insignificant. Consequently, the bit error rate (BER) performance does not improve very much. Moreover, RAKE reception increases the complexity of the receivers; therefore RAKE reception combined with coherent combining is not always beneficial.

6.6 Comparison with receiver diversity

To do a fair comparison we assume an uncorrelated RX array with M antennas, in which each antenna extracts the signal from its strongest path. Then the array is followed by a maximal ratio combiner. Here the system utilizes a single TX antenna which is operating with power E. The correlator output from the n^{th} RX antenna is given by

$$r_n = \int_{jT_b}^{(j+1)T_b} r_n(t) \times b_T(t - \tau_{0,n}^0)_{PPM} dt \ , \tag{6.21}$$

where $r_n(t)$, the received signal of n^{th} antenna is given by

$$r_n(t) = \sum_{u=0}^{Nu-1} \sum_{l=0}^{L-1} h_{l,n}^u \times v_u \left(t - \tau_{l,n}^u \right)_{PPM} + n(t). \tag{6.22}$$

$h_{l,n}^u, \tau_{l,n}^u$ are the corresponding channel parameters related to the n^{th} receiver antenna. The corresponding decision metric ζ from MRC is, $\sum_{n=0}^{M-1} h_{0,n}^0 \times r_n$. Therefore, the SIR in a multi receiver scheme becomes

$$SIR_{multiRx} = \frac{EN_s^2 \sum_{n=0}^{M-1} (h_{0,n}^0)^2}{\sigma^2 + \sigma_I^2}, \tag{6.23}$$

where σ_I^2 is the mean square value of the interference component in r_n. Here we assume that all the interference components are independently and identically distributed. This mean square value will be equal to that of the single antenna scheme, and hence equal to that of the TX diversity scheme. If the values of $h_{0,n}^0, h_{0,m}^0$ are close to each other then,

$$\sum_{n=0}^{M-1} (h_{0,n}^0)^2 \simeq \frac{1}{M} \left[\sum_{m=0}^{M-1} | \ h_{0,m}^0 \ | \right]^2, \tag{6.24}$$

and hence (6.18) and (6.23) will be nearly equal.

6.7 Variance of the MAI

Throughout sections 6.4 to 6.6, the variance of interference was given the same notation σ_I^2 though it had slightly different definitions. This is because the numerical values of σ_I^2 can be shown equal.

6.7.1 Proposed scheme

Let I_m is the interference component from the m^{th} transmit antenna without power scaling, i.e.;

$$I_m = \int_{jT_b}^{(j+1)T_b} \left[\sum_{u=0}^{Nu-1} \sum_{\substack{l=0 \\ (l=1 \; if \; u=0)}}^{L-1} \widehat{h_{l,m}^{u}} \times v_u^{'} \left(t - \widehat{\tau_{l,m}^{u}} \right) \right] b_T^{'}(t)_{PPM} \, dt \qquad (6.25)$$

We assume that the transmit antennas are in equal distance from the desired user and their radiation scattering is uncorrelated. Further, we assume all the I_m components are identically and independently distributed with zero mean (since 0°, 180° phases are equi-probable in channel scattering ($E(I_M) = 0,$). Therefore,

$E(I_0^2) = E(I_1^2) = ... = E(I_{M-1}^2) = \sigma_T^2$, (σ_T^2 is a temporary variable) but the total interference is given by

$$I = \int_{jT_b}^{(j+1)T_b} \left[\sum_{m=0}^{M-1} \sum_{u=0}^{N_u-1} \sum_{\substack{l=0 \\ (l=1 \; if \; u=0)}}^{L-1} \widehat{h_{l,m}^{u}} \times v_u^{'} \left(t - \widehat{\tau_{l,m}^{u}} \right)_{PPM} \right] b_T^{'}(t)_{PPM} \, dt \qquad (6.26)$$

$$= \sum_{m=0}^{M-1} I_m$$

Thus, $E(I^2) = \sum_{m=0}^{M-1} E(I_m^2) = M\sigma_T^2$.

This is when the transmitting pulse energy is E. When each antennas transmit power is scaled down by M, $E(I^2)$ will also be scaled down by M. Thus $E(I^2) = \sigma_I{}^2 = \sigma_T^2$. It should be noted that σ_T^2 would be the variance of interference in a single antenna scheme.

6.7.2 Maximum ratio RAKE combiner

Let $I_r, (r = 0,1,2...M-1)$ denote the interference component from the r^{th} finger. We assume I_r are independent (since the delays are independent and random), where

$$I_r = \int_{jT_b}^{(j+1)T_b} \left[\sum_{u=0}^{N_u-1} \sum_{\substack{l=0 \\ l=1 \, if \, u=0}}^{L-1} h_{l,0}^{u} \times v_u\left(t - \tau_{l,0}^{u}\right)_{PPM} \right] b_T(t - \tau_{r,0}^{0})_{PPM} \, dt \,. \quad (6.27)$$

But, (6.25) and (6.27) are statistically identical, therefore $E({I_r}^2) = {\sigma_T}^2 = {\sigma_I}^2$.

Thus, the variance of total interference is,

$$\begin{aligned} \sigma_{MRRC}^2 &= \sum_{r=0}^{M-1} (h_{r,0}^{0})^2 E({I_r}^2) \\ &= \sigma_I^2 \sum_{r=0}^{M-1} (h_{r,0}^{0})^2 \end{aligned} \quad . \quad (6.28)$$

But,

$$\begin{aligned} SIR_{MRRC} &= \frac{EN_s^2 \left[\sum_{r=0}^{M-1} (h_{r,0}^{0})^2 \right]^2}{\sigma^2 \sum_{r=0}^{M-1} (h_{r,0}^{0})^2 + {\sigma_I}^2 \sum_{r=0}^{M-1} (h_{r,0}^{0})^2} \\ &= \frac{EN_s^2 \left[\sum_{r=0}^{M-1} (h_{r,0}^{0})^2 \right]}{\sigma^2 + {\sigma_I}^2} \end{aligned} \quad (6.29)$$

6.7.3 Multi Rx scheme

Let I_n denote the interference component generated by the n^{th} Rx antenna. We assume that I_n's are independent. I_n is given by

$$I_n = \int_{jT_b}^{(j+1)T_b} \left[\sum_{u=0}^{N_u-1} \sum_{\substack{l=1 \\ l=1 \, if \, u=0}}^{L-1} h_{l,n}^{u} \times v_u\left(t - \tau_{l,n}^{u}\right)_{PPM} \right] b_T(t - \tau_{r,n}^{0})_{PPM} \, dt \, . \qquad (6.30)$$

It is reasonable to assume that eq (6.27) and (6.30) are statistically identical. Therefore,

$E(I_n{}^2) = \sigma_I{}^2 = \sigma_T{}^2$. Therefore $SIR_{multiRx}$ is given by

$$SIR_{multRx} = \frac{E\left[\sum_{n=0}^{M-1} (h_{0,n}^{0})^2\right]^2}{\sigma^2 \sum_{n=0}^{M-1} (h_{0,n}^{0})^2 + \sigma_I{}^2 \sum_{n=0}^{M-1} (h_{0,n}^{0})^2} \qquad (6.32)$$

$$= \frac{E\left[\sum_{n=1}^{M} (h_{0,0}^{0})^2\right]}{\sigma^2 + \sigma_I{}^2}$$

6.8 Simulation results

Performances of the different schemes discussed are evaluated and compared through Monte-Carlo simulations. The channel model, which is presented in 2.2 is used in the simulations, the channel parameters are selected according to CM2 [9].

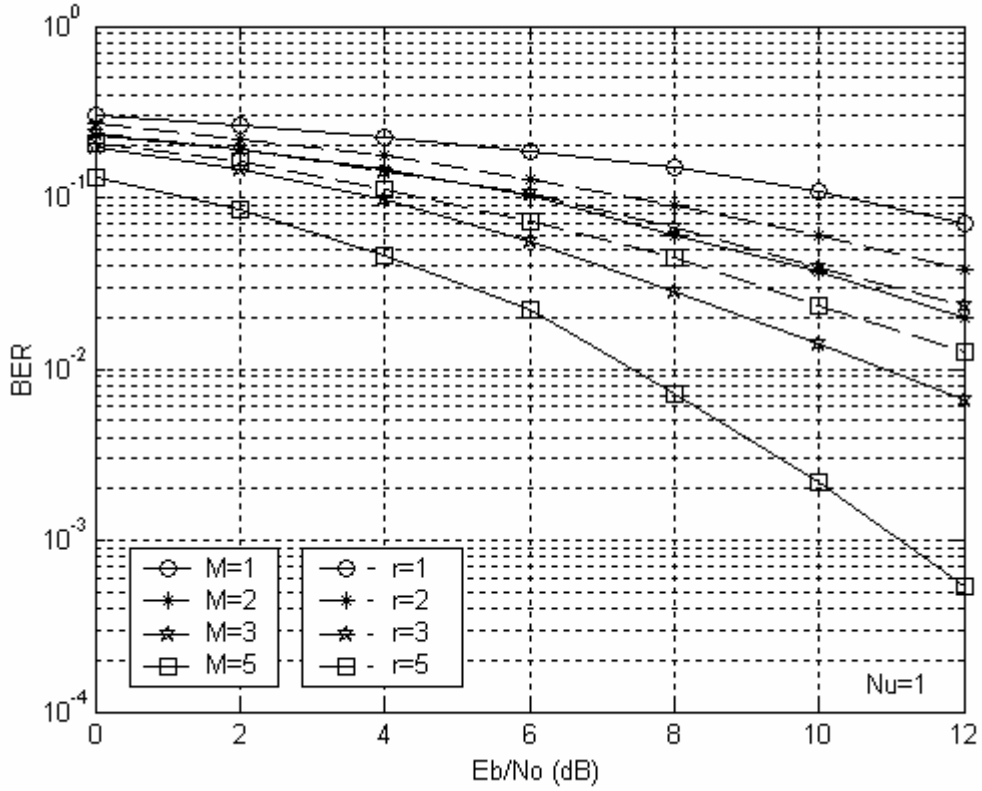

Fig. 6.4 Proposed scheme and RAKE receiver compared in singleuser environment, (r -number of rake fingers).

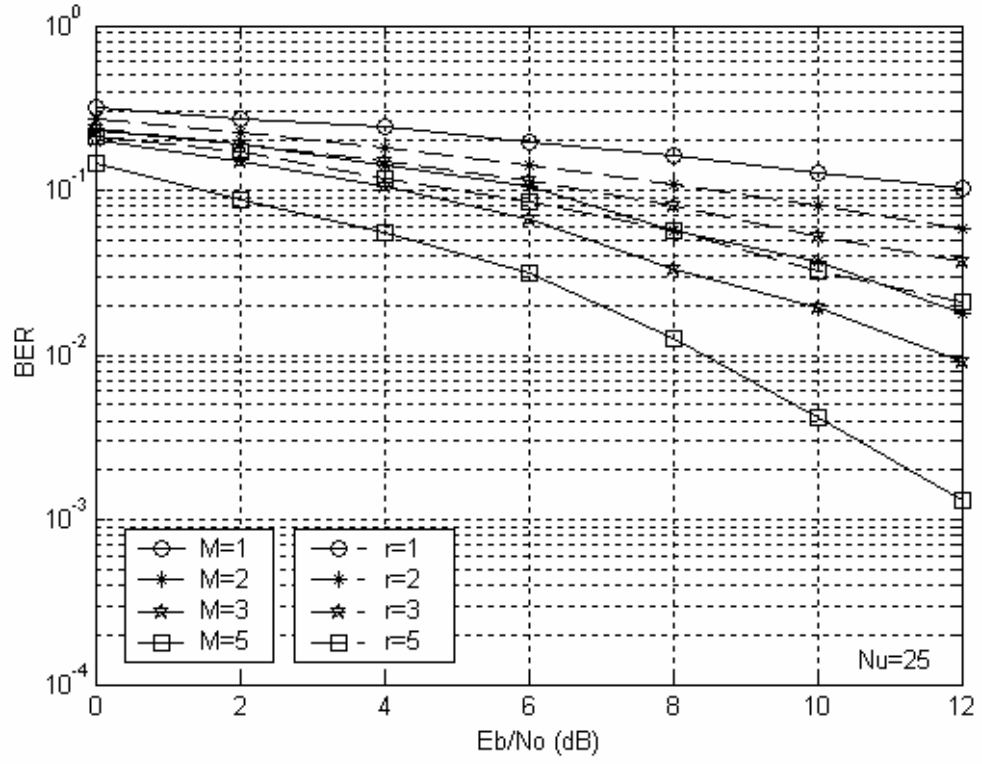

Fig. 6.5 Proposed scheme and RAKE receiver compared in multiuser environment, (r -number of RAKE fingers).

Fig. 6.4. and Fig. 6.5 show the comparison of the performance of the proposed transmitted diversity scheme with single correlator receiver against conventional RAKE receiver performance with single transmitter. In the proposed scheme the performance is improved significantly. In addition, the complexity of the conventional RAKE receiver is proportional to the number of RAKE fingers used [46].

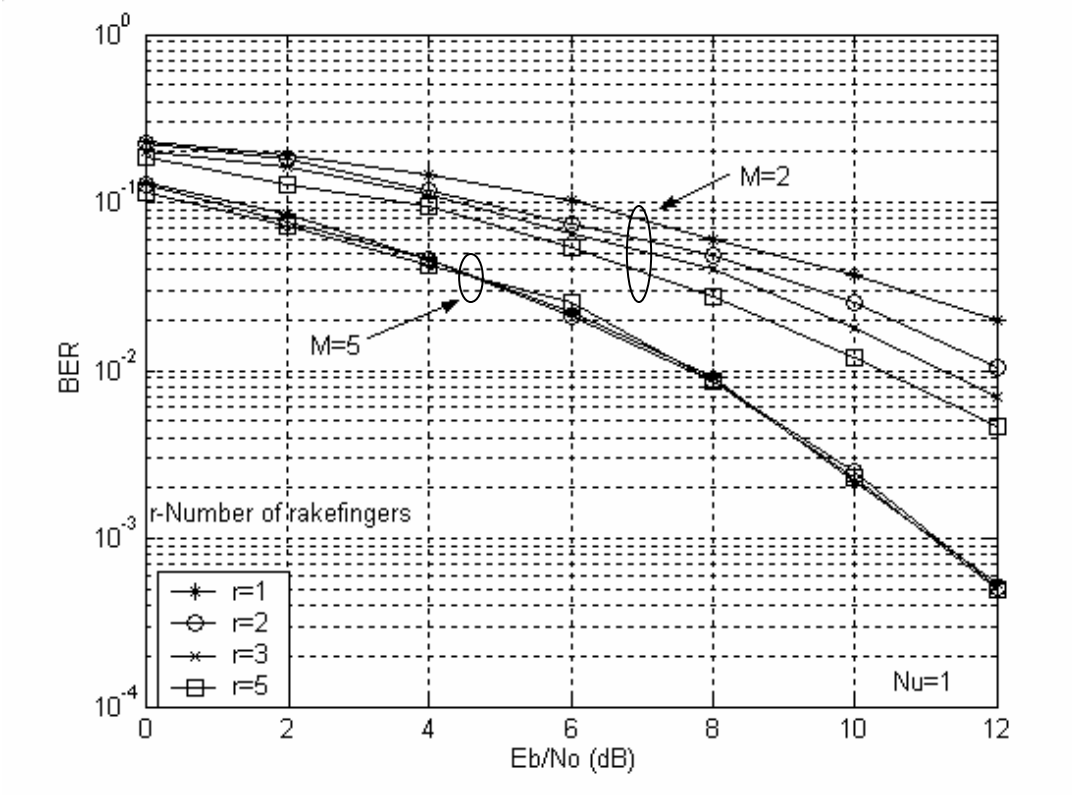

Fig. 6.6 Performance of coherent combining with RAKE reception in singleuser environment.

Fig. 6.6 and Fig. 6.7 show the variation in performance by employing RAKE reception to the proposed scheme. It can be observed that there is not much improvement in performance when the number of TX antennas is large (eg. 5). This is due to the comparatively large gain of the combined path (in average it will be M times larger than the next strongest path in magnitude). However, for two transmitter

case, employing RAKE reception with delay tuning (coherent combining) can be considered if one can trade off the complexity for performance.

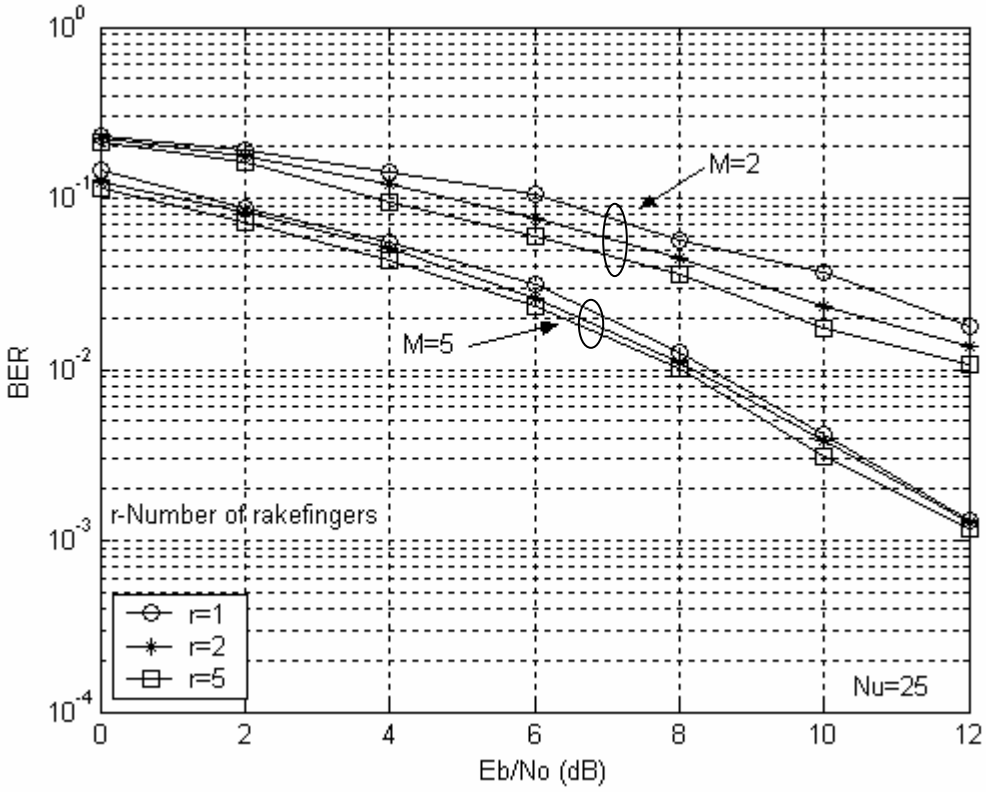

Fig. 6.7 Performance of coherent combining with RAKE reception in multiuser environment.

Fig. 6.8 and Fig. 6.9 show the interesting results, where the proposed TX diversity scheme is compared with RX diversity scheme. As we described in section 6.6, both shows nearly similar performance even in a multiuser multipath environment. The complexity in receiver diversity is proportional to the number of RX antennas employed, contrastingly the proposed transmit diversity scheme has a single correlator receiver structure.

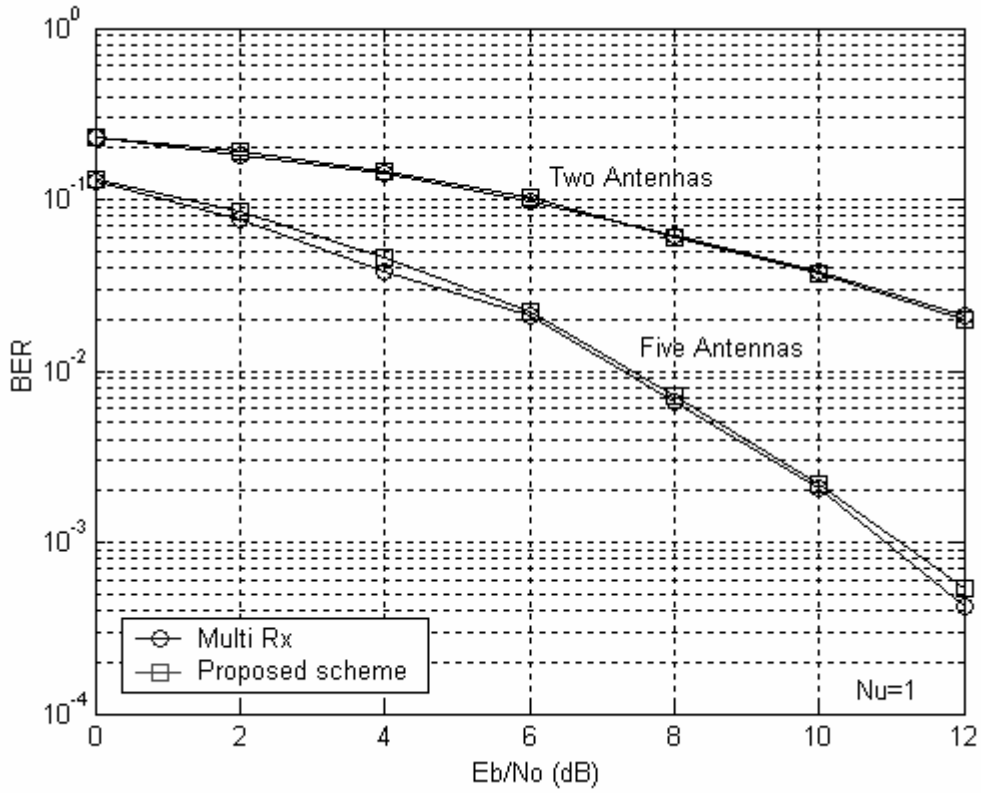

Fig. 6.8 Performance of multi-RX antennas compared with coherent combining in singleuser environment.

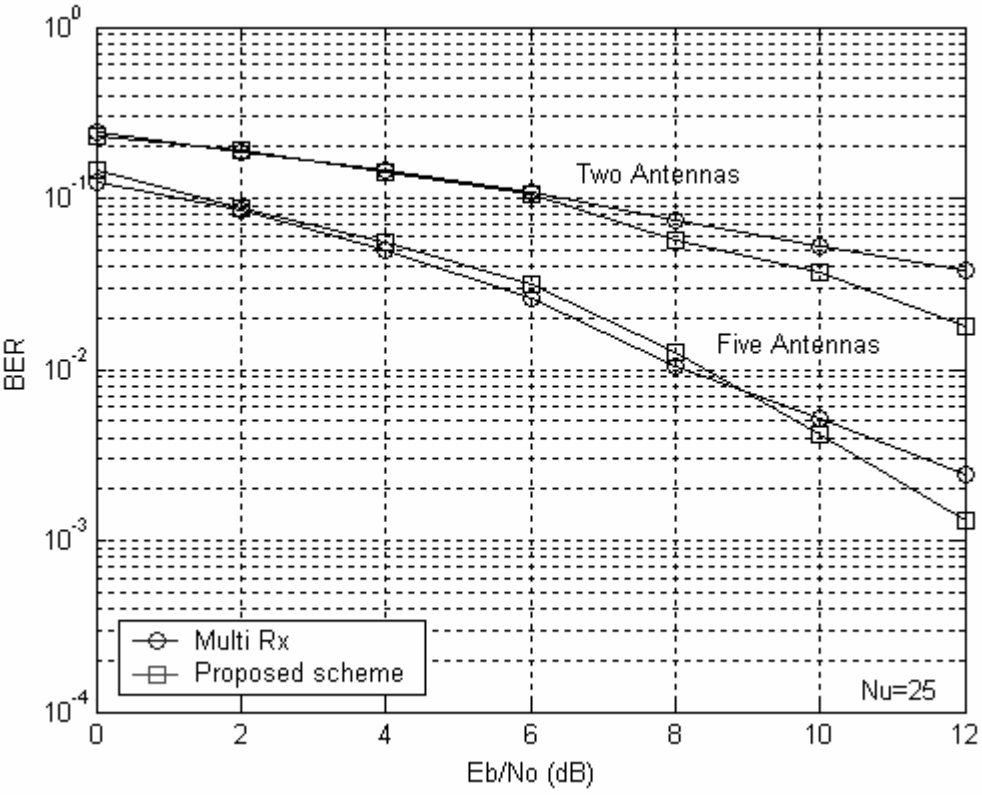

Fig. 6.9 Performance of multi-RX antennas compared with coherent combining in multiuser environment

The main advantage in coherent combining is, the signals from different antennas are combined in space before they enter the correlator module. On the other hand, either in a conventional RAKE receiver or in a multi RX MRC combiner, combining takes place after the correlators, this increases the noise power.

This coherent combining scheme requires feedback information of the channel parameter estimates. The feedback process will anyhow reduce the throughput of the uplink slightly, but this is expected to be a fractional reduction as the channel is quasi static in general. Quasi static channel assumption is valid in an indoor environment [12]. Where the moving scatterers are mainly human bodies and the average mobility of scatterers and the average number of moving objects are not large in an indoor channel. Moreover, mobility of the devices are also very low as they are likely to be placed on tables or held in pockets, or carried in hands. Therefore it is possible to transmit and receive more number of data frames with the current channel estimates. In addition to that the transmitter only needs the sign information of the path gains and the relative time shifts between paths. Therefore, the feed back process will only have a fractional reduction in uplink throughput. The level of timing precision in the hardware required for coherent combining is similar to that needed in the RAKE fingers in synchronizing the correlators with the delayed paths.

6.9 Conclusion

The performance of coherent combining based transmit diversity scheme is compared with conventional RAKE receiver and receiver diversity schemes. RAKE

receiver and multiple RX increase the complexity and hence the cost of the receivers. The proposed scheme operates with only a single correlator and performs significantly better than conventional RAKE receiver and equally to the multi RX receiver in multipath multiuser environments.

We also discussed combining RAKE reception with coherent combining. It is shown that this method is relatively less advantageous. The reason is that the relative improvement by adding a RAKE finger is very small due to the large amount of energy already present in the coherently combined path. However for a 2 antenna scheme it may bring a moderate improvement.

CONCLUSIONS AND FUTURE WORKS

This chapter presents the conclusions and some remarks of this work. Furthermore, it presents some suggestions and identifies few problems for future research work.

7.1 Conclusions

The contributions of this research work are two fold: One is theoretical performance evaluation and the other is performance improvement techniques.

An exact method for statistically modeling the MAI is introduced for TH-PPM, TH-PAM and DS-PAM in AWGN channels. We have proposed a scheme to model the interference from a single user and have extended it to model the multiuser interference by assuming that the interferers are independent. In previous works, partially asynchronous channel access is assumed and the interferences within each frame are assumed to be independent. These drawbacks are eliminated in our proposed solutions. The interference is modeled directly from basic principles using the geometric properties of the UWB-IR signals.

This modeling is then used to derive exact performances of various UWB systems in terms of BER using the widely known characteristic function technique. This CF technique has an advantage of simplifying the calculations when a number of independent variables are summed together to form the decision variable. Wherever

possible, symmetric property of the interference is used to simplify the formulas and express them in real function forms. It is also pointed out in this thesis that this symmetry is not available for binary non-orthogonal PPM modulation if the mono-pulse shape is not symmetric. In such cases the complex form of the BER equations should be used.

In Chapter 4 it is shown that the modeling of MAI in AWGN channels can be used to develop the formulas for evaluating the system BER performance in multipath fading channels. The BER for a single correlator receiver is accurately derived in fading multipath channels. Although we have considered TH-PPM systems in this chapter, it should be noted that the same method can be used to derive the BER formulas for the other forms of modulations (PAM, OOK) and multiple access schemes (DS).

In chapter 4, on the course of these derivations, we have developed an accurate method to evaluate the CF of a log normal variable. This method uses a combination of three numerical integration approximations based on the range of the mean (μ) of the lognormal random variable.

The problem of RAKE receiver performance is not addressed here due to its high complexity. The complexity arises especially in handling the lognormal variables and due to the non uniform PDP of the channel.

We concentrate on binary modulations in chapter 3 and chapter 4, and look in to M-ary systems in chapter 5. Exact modeling of MAI for M-ary TH-PPM and TH-PAM is presented. Using this model the SER of an M-ary TH-PAM system is derived.

Though an exact model for MAI is available, deriving the exact SER is complex for an M-ary TH-PPM system due to the receiver structure. Therefore, an upper bound and an approximate formula for the SER are derived for an M-ary TH-PPM system.

In chapter 6 a novel technique is proposed to improve the UWB-IR system performance. This is based on the idea of coherent combining, i.e. combining the signals in space before they enter the Rx antenna rather than combining them in the receiver as electronic signals. This method prevents the multiplication of noise energy which occurs when multiple correlators (RAKE fingers) are used to extract the energy from multipaths. The proposed scheme performs significantly better than conventional RAKE receivers and performs equally to multi-Rx schemes in typical UWB environments while making the receiver comparatively much simple.

Some of the results from these works can be found in [30], [38] and [53-56].

7.2 Future works

In the context of this research the following problems can be identified as future research problems.

It should be noted that the modeling of MAI and BER derivation are possible through similar fashion for binary systems like TH-OOK, DS-OOK and DS-PPM, which are not addressed in this thesis. It is easy to handle OOK as a variation of PAM modulation in both TH and DS schemes. Similar extension is possible also for M-ary DS-PAM system.

In order to handle the RAKE receiver problem accurately, instead of using the exact model of multiple access interference, it will be necessary to look for an approximate probabilistic model for the total interference. Such a model can be obtained from simulation or measurement data, but it should be capable of reflecting the effects of modulation parameters and pulse shape accurately. Once such a model is available for MAI, then the next problem is to find the distribution of the weighted sum of similar MAI variables.

Apart from the accuracy of the formulas for estimating the performance, another important issue is the computational efficiency of the methods. In some cases accuracy can be compromised for computational efficiency. Therefore, a comparison of different approximate methods is required in proposing a solution for the RAKE receiver problem.

In evaluating the performance of the proposed coherent combining scheme, it was assumed that perfect channel information is available. But, it is important to know the effect of the estimation errors on the system performance. Furthermore, it is also important to investigate the level of accuracy required in parameter estimation, which in turn will have a direct impact on the data rate of the feedback path. In order to reduce the computation load at the receiver and the feedback data rate, adaptive channel parameter adjustment algorithms can be used.

The proposed technique of coherent combining is suitable for applications in secure or covert communications. One example is that an array of antennas can be used to focus the signals on a ‘friendly user’ while avoiding the others. Another area is

security, where such a focusing array can be used to detect unauthorized motion in a room. An array can be focused on (tuned) to a particular Rx point which can be LOS / NLOS, and the tuning could be disturbed due to a movement of an object which will results in lower signal strength at the Rx and hence the movement can be detected.

REFERENCES

[1] F. Ramirez-Mireles, “Multiple-access with ultra-wideband impulse radio modulation using spread spectrum time hopping and block waveform pulse position modulated signals ‘, *PhD Dissertation,* 1998.

[2] R. Scholtz, “Multiple access with time-hopping impulse modulation”, *Military Communications Conference, MILCOM '93*, vol.2, Oct. 1993, pp. 447 -450.

[3] M.Z. Win, and R.A. Scholtz, “Impulse radio: how it works”, *IEEE Communications Letters*, Vol. 2 , Iss. 2 , Feb. 1998, pp.36 – 38.

[4] M.Z. Win, and R.A. Scholtz, “Ultra-wide bandwidth time hopping spread-spectrum impulse radio for wireless multiple-access communications”, *IEEE Trans. Comm.*, Vol.48., April 2000, pp.679-689.

[5] FCC First report and order regarding Ultra wideband transmission and systems, http://ftp.fcc.gov/Bureaus/Engineering_Technology/Orders/2002/fcc02048.pdf, April, 2002.

[6] M.L. Welborn, “System considerations for ultra-wideband wireless networks”, *IEEE Radio and Wireless Conference*, 2001, Aug. 2001, pp. 5 – 8.

[7] K. Siwiak, “Ultra-wide band radio: introducing a new technology”, *Proc. IEEE VTC 2001 Spring, Vol. 2* , May 2001, pp. 1088 -1093.

[8] R.J. Fontana, “Recent system applications of short-pulse ultra-wideband (UWB) technology”, *IEEE Transactions on Microwave Theory and Techniques,* Vol. 52 , Iss. 9, Sept. 2004 , pp. 2087 – 2104.

[9] IEEE P802.15 Working Group for Wireless Personal Area Networks (WPANs), “Channel Modeling Sub-committee Report Final”, Dec. 2002.

[10] A. F. Molisch, J. R Foerster, and M. Pendergrass, “Channel models for Ultrawideband Personal Area Networks”, *IEEE Wireles Comm. Mag.*,Dec. 2003.

[11] R.J.-M. Cramer, R.A. Scholtz, and M.Z. Win, “Evaluation of an ultra-wide-band propagation channel”, *IEEE, Transactions on Antennas and Propagation,* Vol. 50 , Iss. 5 , May 2002, pp. 561 – 570.

[12] A. Saleh, and R. Valenzuela, “A Statistical Model for Indoor Multipath Propagation”, *IEEE J. Select. Areas. Comm.*, Vol. 5, Feb 1987, pp. 128 -137.

[13] Foerster, J., and Q. Li, UWB Channel Modeling Contribution from Intel, Available at grouper.ieee.org/groups/802/15/pub/2002/Jul02/02279r0P802-15_SG3a-Channel-Model-Cont-Intel.doc (June 2002).

[14] D. Cassioli, M.Z. Win, A.F. Molisch, “The ultra-wide bandwidth indoor channel: from statistical model to simulations”, *IEEE Journal on Selected Areas in Communications*, Vol. 20 , Iss. 6 , Aug. 2002, pp. 1247 – 1257.

[15] J. A. Ney da Silva and M. L. R. de Campos, "Performance Comparison of Binary and Quaternary UWB Modulation Schemes," *Proc IEEE Conf. on GLOBECOM '03*, pp. 789 - 793, 1-5 Dec.2003.

[16] J. Zhang, T. D. Abhayapala, and R. A. Kennedy, "Performance of ultra-wideband correlator receiver using Gaussian monocycles," *Proc IEEE Conf. on ICC '03*, pp. 2192 -2196, Vol. 3, May 2003.

[17] Guangrong Yue, Lijia Ge, and Shaoqian Li, "Performance of UWB time-hopping spread-spectrum impulse radio in multipath environments," *Proc IEEE Conf. on VTC 2003-Spring*, pp. 1644 - 1648 , Vol. 3, April 2003 .

[18] Huaping Liu, "Error performance of a pulse amplitude and position modulated ultra-wideband system over lognormal fading channels," *IEEE Commun. Lett.*, Vol. 7, pp. 531 - 533, Nov 2003.

[19] Huaning Niu, J. A. Ritcey, and Hui Liu, "Performance of UWB RAKE receivers with imperfect tap weights," *IEEE Conf. on Acoustics, Speech, and Signal Processing*, 2003, pp. IV - 125-8, Vol. 4, April 2003 .

[20] E. R. Bastidas-Puga, F. Ramirez-Mireles, and D. Munoz-Rodriguez, "Performance of UWB PPM in residential multipath environments," *Proc IEEE Conf. on VTC 2003-Fall*, Vol. 4, pp. 2307 - 2311, Oct. 2003 .

[21] S. Gaur and A. Annamalai, "Improving the range of ultrawideband transmission using RAKE receivers," *Proc IEEE Conf. on VTC 2003-Fall*, Vol. 1, pp. 597 - 601, Oct. 2003 .

[22] J. D. Choi and W. E. Stark, "Performance of ultra-wideband communications with suboptimal receivers in multipath channels," *IEEE Selected Areas Commun*., Vol. 20, pp. 1754 -1766, Dec 2002.

[23] D. Cassioli, M. Z. Win, F. Vatalaro, and A. F. Molisch, "Performance of low-complexity RAKE reception in a realistic UWB channel," *Proc IEEE Conf. on ICC 2002*, Vol. 2 , 28 April-2 May 2002 , pp. 763 - 767 .

[24] J. D. Choi and W. E. Stark, "Performance analysis of RAKE receivers for ultra-wideband communications with PPM and OOK in multipath channels," *Proc IEEE Conf. on ICC 2002*, Vol. 3, 28 April-2 May 2002 , pp. 1969 – 1973.

[25] F. Ramirez-Mireles, "On the performance of ultra-wide-band signals in Gaussian noise and dense multipath," *IEEE Trans. On Veh. Technol*., Vol. 50, pp. 244 -249, Jan 2001.

[26] G. Durisi and S. Benedetto, "Performance evaluation and comparison of different modulation schemes for UWB multiaccess systems," *Proc IEEE Conf. on ICC '03*, pp. 2187 - 2191, Vol. 3, May 2003

[27] F. Ramirez-Mireles, "Performance of ultrawideband SSMA using time hopping and M-ary PPM," *IEEE Selected Areas Commun.*, Vol. 19, pp. 1186 - 1196, June 2001 .

[28] A. R. Forouzan, M. Nasiri-Kenari, and J. A. Salehi, "Performance analysis of ultrawideband time-hopping code division multiple access systems: uncoded and coded schemes," *Proc IEEE Conf. on ICC 2001*, Vol. 10, 11-14 June 2001, pp. 3017 - 3021.

[29] V. Venkatesan, Huaping Liu, C. Nilsen, R. Kyker, and M. E. Magana, "Performance of an optimally spaced PPM ultra-wideband system with direct sequence spreading for multiple access," *Proc IEEE Conf. on VTC 2003-Fall* , Vol. 1, pp. 602 - 606 ,Oct. 2003 .

[30] S. Niranjayan, A. Nallanathan and B. Kannan, "Delay Tuning Based Transmit Diversity Scheme for TH-PPM UWB: Performance with RAKE Reception and Comparison with Multi RX Schemes", *Proc Joint UWBST and IWUWBS 2004*, May 2004.

[31] G. Durisi and G. Romano, "On the validity of Gaussian approximation to characterize the multiuser capacity of UWB TH PPM," *Proc IEEE Conf. on Ultra Wideband Systems and Technologies 2002*, May 2002, pp. 157 - 161.

[32] A. R. Forouzan, M. Nasiri-Kenari, and J. A. Salehi, "Performance analysis of time-hopping spread-spectrum multiple-access systems: uncoded and coded schemes," *IEEE Trans. Wireless Commun*. Vol. 1, pp. 671 - 681, Oct. 2002 .

[33] K. A. Hamdi and Xuanye Gu, "On the validity of the gaussian approximation for performance analysis of TH-CDMA/OOK impulse radio networks," *IEEE Conf. on VTC 2003-Spring*, pp. 2211 - 2215, April 2003 .

[34] B. Hu, and N.C Beaulieu, “Exact bit error rate analysis of TH-PPM uwb systems in the presence of multiple-access interference”, *IEEE Comms. Lett*., Vol. 7, Iss. 12, Dec. 2003 pp. 572 – 574.

[35] M. Sabattini, E. Masry, and L. B. Milstein, "A non-gaussian approach to the performance analysis of UWB TH-BPPM systems," *Proc EEE Conf. on Ultra Wideband Systems and Technologies*, Nov 16-19, 2003, pp. 52 - 55.

[36] G. Durisi and S. Benedetto, "Performance evaluation of TH-PPM UWB systems in the presence of multiuser interference," *IEEE Commun. Lett*., Vol. 7, pp. 224 -226, May 2003.

[37] K. A. Handi and Xuanye Gu, "Bit error rate analysis for TH-CDMA/PPM impulse radio networks," *Proc IEEE Conf. on Wireless Communications and Networking*, 2003., pp. 167 - 172 , Vol. 1, 16-20 March 2003 .

[38] S. Niranjayan, A. Nallanathan and B. Kannan, “A New Analytical Method for Exact Bit Error Rate Computation of TH-PPM UWB Multiple Access Systems”, *PIMRC2004*, September 2004.

[39] M.K Simon, and M.S Alouini, Digital communication over fading channels - A unified approach to performance analysis, John wiley & sons, inc., USA, 2000.

[40] N. C. Beaulieu, A. A. Abu-Dayya, and P. J. McLane, “Estimating the Distribution of a Sum of Independent Lognormal Random Variables”, *IEEE Comms. Trans.*, Dec. 1995, pp. 2869-2873.

[41] N. C. Beaulieu, and Q. Xie, “An Optimal Lognormal Approximation to Lognormal Sum Distributions”, *IEEE Trans. On Vech. Tech*, April 2004, pp. 479 - 489.

[42] Roy B. Leipnik, “On lognormal Random Variables: I-The Characteristic Function”, *J. Austral. Math. Soc.*, Ser. B 32(1991), 1991, pp. 327-347.

[43] M. S. Alouini, and A. J. Goldsmith, “A Unified Approach for Calculating Error Rates of Linearly Modulated Signals Over Generalized Fading Channels”, *IEEE Comms. Trans.*, Sep. 1999, pp. 1324-1334.

[44] http://mathworld.wolfram.com/

[45] http://www.efunda.com/math/num_integration/findgausshermite.cfm

[46] M.Z. Win, and R.A. Scholtz, "Characterization of ultra-wide bandwidth wireless indoor channels: a communication-theoretic view", *IEEE J. Select. Areas. Comm.*, Vol. 20, No 9, Dec 2002, pp. 1613- 1627.

[47] M.Z. Win, Z.A. Kostic, "Impact of spreading bandwidth on RAKE reception in dense multipath channels", *IEEE J. Select. Areas. Comm.*, Vol. 17, No. 10, Oct 1999, pp. 1794 - 1806.

[48] M.Z. Win, G. Chrisikos, N.R. Sollenberger, "Performan-ce of RAKE reception in dense multipath channels: implications of spreading bandwidth and selection diversity order", *IEEE J. Select. Areas. Comm.*, Vol. 18, No. 8, Aug 2000, pp. 1516 - 1525.

[49] S.M. Alamouti,; "A simple transmit diversity technique for wireless communications", *IEEE J. Select. Areas Comm.*, Vol. 16, Oct. 1998, pp.1451 - 1458.

[50] Liuqing Yang, and G.B. Giannakis, "Space-time coding for impulse radio", *Digest of Papers, IEEE Conf., in Ult. Wid. Sys. and Tech.*, May 2002, pp 235 - 239.

[51] E.E. Funk, and C.H. Lee, "Free-space power combining and beam steering of ultra-wideband radiation using an array of laser-triggered antennas", *IEEE Tran., Microwav. Th., and Tech.*,Vol. 44, Nov. 1996, pp. 2039 - 2044.

[52] R. Hackett, C.D. Taylor, D. Mclemore, H. Dogliani, W.A. Walton, III; and A.J. Leyendecker, "Selective targeting: developing a space time array to increase the peak power delivered to a localized region in space", *IEEE Int. Symp., Anten. and Prop. Soc.*, July 1999, Vol. 2, pp.1000 – 1003.

[53] S. Niranjayan, A. Nallanathan and B. Kannan, "An Adaptive Transmit Diversity Scheme Based on Spatial Signal Combining for TH-PPM UWB", *ISSSTA 2004*, Aug 2004.

[54] S. Niranjayan, A. Nallanathan and B. Kannan, "Exact Modeling of Multiple Access Interference and BER Derivation for TH -PPM UWB", *WCNC 2005*, Accepted for publication.

[55] S. Niranjayan, A. Nallanathan and B. Kannan, "Modeling of Multiple Access Interference and SER Derivation for M-ary TH- PAM /PPM UWB Systems", *VTC Spring 2005*, Accepted for publication.

[56] S. Niranjayan, A. Nallanathan and B. Kannan, "Modeling of Multiple Access Interference and BER Derivation for TH and DS UWB Multiple Access Systems", *IEEE Transactions on Wireless communications*, Aug. 2004. Submitted.